DOE/BC/10331-13
Distribution Category UC-92a
PRRC 84-10

# Displacement of Oil by Carbon Dioxide

Final Report

F.M. Orr, Jr. and J.J. Taber
Principal Investigators

New Mexico Petroleum Recovery Research Center
New Mexico Institute of Mining and Technology
Socorro, New Mexico

Contributors:

I.M. Bahralolom
R.E. Bretz
K.K. Dai
L.L. Larsen
C.L. Lien
M.T. Pelletier
G.J. Ruskauff
M.K. Silva
R.M. Specter
M.A. Taylor
S.L. Welch

Prepared for the U.S. Department of Energy
Under Contract No. DE-AS19-80BC10331

March, 1984

TABLE OF CONTENTS

## LIST OF TABLES

## LIST OF FIGURES

samples with wide pore size distributions and pore connections which generate preferential flow paths.

The theory of the effect of $CO_2$-crude oil phase behavior on displacements in an ideal porous medium is tested by predicting the performance of slim tube displacements from independently measured phase behavior and fluid property data obtained with the continuous multiple contact experiment. The quantitative agreement between prediction and experiment is good enough to suggest that the essentials of $CO_2$-crude oil phase behavior can be modeled with a small number of pseudo-components. Modifications to the simulator to model effects of dendritic and trapped saturations are described. Calculated composition paths for both secondary and tertiary displacements indicate that microscopic limitations to mixing, due to heterogeneity of the rock or to the presence of water, adversely affect local displacement efficiency.

## ABSTRACT

Results of a comprehensive research effort to identify, investigate and quantify factors which influence $CO_2$ flood performance are presented.

Results of static equilibrium phase behavior experiments for mixtures of $CO_2$ with Wasson crude and Wasson oil containing varying amounts of solution gas are reported for three temperatures, 90, 105 and 120°F. Analysis of the resulting phase diagrams suggests a simple correlation for minimum miscibility pressure (MMP) based on the vapor pressure of $CO_2$, extrapolated if necessary for temperatures above the critical temperature of $CO_2$. Results of phase behavior experiments with the same oil and $CO_2$ contaminated with nitrogen are also reported, and a simple procedure for estimating the effects of changes in system temperature or contamination of the $CO_2$ on MMP is offered.

Results of detailed measurements of phase compositions in $CO_2$-hydrocarbon systems are presented. Partitioning of paraffinic, naphthenic and aromatic hydrocarbons between $CO_2$-rich and oil-rich phases was investigated in continuous multiple contact (CMC) experiments. CMC measurements of phase compositions and densities for the quaternary system $CO_2$-methane-butane-decane and several associated binary and ternary systems at 160°F are reported and compared with phase behavior calculated with the Peng-Robinson equation of state. Predictions of liquid-liquid and liquid-liquid-vapor phase behavior made with the equation of state are also compared with experimental observations.

A design of a high pressure holder for an oscillating quartz crystal is described. The crystal holder is part of equipment for measurement of phase viscosities at high pressure. Results of test measurements for fluids for which viscosity data are available indicate that the technique allows very accurate viscosity measurements over a wide range of viscosities.

An apparatus is described in which displacement of oil from pore networks etched in glass by $CO_2$ at high pressure can be observed visually. Results of a series of immiscible, first contact miscible and multiple contact miscible, secondary and tertiary $CO_2$ and nitrogen floods are reported. Observations of tertiary miscible $CO_2$ displacements of a crude oil indicate that $CO_2$ contacts oil much more efficiently if the porous medium is oil-wet. Direct observations also indicate that $CO_2$ can diffuse through water to contact trapped oil. A new technique for measurement of diffusion coefficients for $CO_2$ in water and oil at high pressure is described.

Experimental equipment for on-line measurement of effluent fluid compositions in one- and two-phase, steady-state displacements in reservoir core samples is described. Results of single-phase miscible displacements with fluids of matched density and viscosity for seven core samples are reported. Effluent composition data were interpreted using the Coats-Smith model. Thin sections of the core samples were examined in an attempt to relate microscopic heterogeneity to average displacement behavior on the core scale. Early breakthrough of injected fluid was found to occur for rock

# 1. INTRODUCTION

The performance of a $CO_2$ flood at field scale is the result of a complex set of interactions of the physical chemistry of $CO_2$-crude oil mixtures with generally unstable, multiphase flow in reservoir rocks. The importance of the phase behavior of $CO_2$-crude oil mixtures in the generation of high local displacement efficiency is by now well established, at least in the simple flow setting of a slim tube displacement. Extraction of hydrocarbons from the oil by a $CO_2$-rich phase generates mixtures which then can displace nearly all of the oil. Flows in reservoir rocks are significantly more complex, however. Rocks may be much more heterogeneous than sand or bead packs at scales ranging from the pore level to interwell distances. Both the heterogeneity of the pore structure and the presence of water in a portion of the pore space may alter mixing of $CO_2$ and oil in such a way as to change the compositions of the resulting $CO_2$-rich and oil-rich phases. Because local displacement efficiency is sensitive to the composition path of fluids in the porous medium, changes in mixing behavior may also affect process performance.

This report describes results of a comprehensive research effort aimed at quantifying the effects of phase behavior and mixing during flow in reservoir rocks. The approach taken here is to perform experiments in which relevant physical effects are isolated so that the quantitative effects of a particular physical mechanism can be measured and the experiment interpreted unambiguously. Effects of interactions of process mechanisms are then studied by numerical simulation of the displacement process. Accordingly, details of three parallel investigations are reported: phase behavior and fluid property measurements, high pressure flow visualization experiments, and miscible displacement experiments in reservoir cores.

In chapter 2, results of an extensive experimental effort to understand the physical chemistry of $CO_2$-crude oil and $CO_2$-hydrocarbon mixtures are summarized. Results of static equilibrium PVT experiments to investigate the effects of changes in system temperature, the amount of solution gas present in the reservoir fluid, and contamination of $CO_2$ by $N_2$ are reported. The phase diagrams obtained are analyzed in terms of the behavior of simpler $CO_2$-alkane mixtures. The analysis of the phase diagrams is used to delineate conditions at which liquid-liquid, liquid-vapor, and liquid-liquid-vapor phase separations occur and to construct a simple, but physically based correlation for the pressure required for efficient displacement of crude oil by $CO_2$ (minimum miscibility pressure).

Also reported in chapter 2 are results of detailed measurements of phase compositions and densities for mixtures of $CO_2$ with synthetic and crude oils. The measurements were made with the continuous multiple contact apparatus developed as part of this and a previous project. The experiments with synthetic oils shed some light on the role of molecular type in $CO_2$-hydrocarbon phase behavior. Calculations, with the Peng-Robinson equation of state, of phase compositions and densities for some of the synthetic systems are compared with available experimental data. In the final section of chapter 2, the development of a viscometer based on an oscillating quartz crystal is described.

In chapter 3, high pressure flow visualization experiments are described which examine displacement events at the pore level in $CO_2$ floods performed in two-dimensional pore networks etched in glass. While the pores in the glass models differ in significant ways from those in rocks, the observations illustrate mechanisms which must operate during flows in reservoir rocks. Secondary and tertiary displacement experiments show clearly how phase behavior, wetting behavior and pore geometry interact to determine local displacement efficiency. The interaction of viscous instability and phase behavior is illustrated, and the fact that $CO_2$ can diffuse through water to reach, swell and recover trapped oil is demonstrated. Design of an experiment to measure diffusion rates through water at high pressure is also described.

Chapter 4 reports results of miscible displacements in reservoir core samples. The experiments are designed to examine the effects of pore structure and the distribution of oil and water in the pore space on mixing between an injected solvent and the fluid in place. Stable, steady-state displacements of both the wetting and nonwetting phases by fluids of matched density and viscosity permit analysis of mixing effects in the absence of effects of phase behavior, fluid property variations, viscous instability and gravity segregation. In the final part of chapter 4, displacement behavior is compared with an analysis of thin sections of the reservoir core material in an attempt to relate displacement performance directly to pore structure.

Chapter 5 reports results of an effort to tie together the experimental investigations of the previous three chapters. Two versions of a one-dimensional process simulator are described. The simpler of the two models flow of up to four phases with volume change on mixing in a uniform porous medium. That simulator is used to predict performance of slim tube displacements based on data from continuous multiple contact experiments. The second models the effects of pore structure heterogeneity and restrictions to mixing caused by the presence of additional water. The more complex model is used to examine the impact of the type of mixing observed in the displacements in reservoir rocks when the effects of phase behavior are also present.

Thus, the research effort described here is a systematic investigation intended to improve understanding of the factors which determine displacement efficiency in a $CO_2$ flood. In particular, it is an attempt to quantify the interactions of phase behavior and flow of multiphase, multicomponent mixtures in realistic porous media. The long-term goal of this work is to improve the accuracy of performance predictions for field-scale $CO_2$ floods. Such predictions are made now, of course, with one of three types of numerical simulators available for simulation of miscible flood processes. However, none of the currently available simulators models all of the factors known to influence flood performance. Miscible simulators (Todd & Longstaff 1972) treat $CO_2$ as completely miscible with oil and model the effects of viscous instability in an empirical way. Compositional simulators (McDonald 1971; Nolen 1973; Kazemi et al 1978; Fussell & Fussell 1977; Coats 1979; Sigmund et al 1979) follow the transport of individual components (or pseudo-components) based on a calculation of the distribution of components between phases using an equation of state or K-value correlations. A hybrid of these two types (Todd 1979) treats $CO_2$ as first contact miscible with the oil above some pressure and models viscous instability as in the miscible simulators, but allows limited component partitioning below the miscibility pressure.

There are fundamental limitations in each of these simulation approaches. The miscible simulators ignore the role of extraction of hydrocarbons from the oil in the generation of high microscopic displacement efficiency. Compositional simulators treat fluids as well mixed in each grid block, a model assumption which neglects the effects of viscous instability. Neither simulator models the effects of restrictions to mixing, addressed in this project, on local displacement efficiency. The difficulty is a fundamental one that stems from the range of scales on which process mechanisms operate in a $CO_2$ flood. Microscopic displacement efficiency is strongly influenced by the transfer of components between phases in a $CO_2$ flood, and in some other enhanced recovery processes. Such transfers require mixing at the pore level, but such mixing is also coupled to the larger scale movements of oil, water and $CO_2$, which determine macroscopic distributions of fluids. Successful development of improved predictive techniques will require that the essential features of physical mechanisms operating at the pore level in reservoir rocks be represented in some average way for use in simulators which represent the reservoir as discrete grid blocks many orders of magnitude larger than the pores. The research effort described here is an attempt to provide the base of understanding of the physical mechanisms required for such representations.

# 2. PHASE BEHAVIOR AND FLUID PROPERTY MEASUREMENTS

Detailed interpretations of flow experiments in which $CO_2$ displaces crude oil require that phase composition and fluid property data be available from independent measurements or from reliable calculations with an equation of state or other representation of phase behavior. For an example of just this sort of interpretation for slim tube displacements, see §5.1. In this chapter, we report results of two experimental investigations of phase behavior. In the first, the volumetric behavior of $CO_2$ and $CO_2$-$N_2$ mixtures with crude oil was measured in standard static equilibrium single-contact phase behavior experiments (Orr et al 1982). The results of those experiments illustrate the effects of increasing temperature, of increasing the amount of solution gas in the oil, and of addition of contaminants in the $CO_2$. They provide additional confirmation that a $CO_2$-rich phase extracts hydrocarbons effectively when its density is high. The results also suggest a simple correlation for minimum miscibility pressures (MMP) in low temperature reservoirs and a procedure for estimation of the effects of contamination of $CO_2$ by $N_2$ or methane.

In the second investigation, phase composition measurements were obtained in a dynamic experiment for both crude oil and well characterized hydrocarbon systems. Comparison of the results gives some indication of the influence of hydrocarbon molecular type on extraction of hydrocarbons by dense $CO_2$. In addition, measured phase compositions are compared with values calculated with the Peng-Robinson equation of state (Peng & Robinson 1976) for binary, ternary and quaternary systems which show liquid-vapor, liquid-liquid and liquid-liquid-vapor separations, with excellent quantitative agreement. Finally, the development and testing of a viscometer based on an oscillating quartz crystal is described. Test measurements for known fluids indicate that the method is a rapid and convenient technique for obtaining viscosity measurements in a high pressure flow system such as the continuous multiple contact experiment.

## 2.1 Static Equilibrium PVT Experiments

### $CO_2$-Wasson Oil Mixtures

A series of single contact phase behavior experiments was performed with crude oil from the Wasson field (Gaines and Yoakum Counties, Texas) in an experimental apparatus described previously (Orr & Taber 1981). The composition of the oil, determined by gas chromatography (Orr & Taber 1982) is given in Table 2.1, along with the composition of gas added to it. Calculated compositions of two recombined oil mixtures, one containing 312 SCF/BBL and the other 602 SCF/BBL, are also given in Table 2.1. Pressure composition (P-X) phase diagrams were determined for the dead oil and the two recombined oils at three temperatures: 90, 105 and 120°F (32, 41 and 49°C). Results of those experiments are given in Figs. 2.1-2.3.

Table 2.1 Compositions of Gas, Oil and Recombined Fluids

| | Gas | Oil | Oil + 312 SCF/BBL | Oil + 602 SCF/BBL |
|---|---|---|---|---|
| $C_1$ | 57.36 | - | 21.33 | 53.03 |
| $C_2$ | 19.89 | - | 7.39 | 18.39 |
| $C_3$ | 16.29 | - | 6.05 | 15.06 |
| $C_4$ | 6.46 | - | 2.41 | 5.98 |
| $C_5$ | - | 5.48 | 3.44 | 0.41 |
| $C_6$ | - | 5.37 | 3.37 | 0.40 |
| $C_7$ | - | 7.40 | 4.65 | 0.56 |
| $C_8$ | - | 12.45 | 7.82 | 0.94 |
| $C_9$ | - | 8.71 | 5.46 | 0.66 |
| $C_{10}$ | - | 6.39 | 4.02 | 0.48 |
| $C_{11}$ | - | 4.59 | 2.88 | 0.34 |
| $C_{12}$ | - | 4.63 | 2.91 | 0.35 |
| $C_{13}$ | - | 3.89 | 2.44 | 0.29 |
| $C_{14}$ | - | 3.58 | 2.25 | 0.27 |
| $C_{15}$ | - | 2.84 | 1.79 | 0.22 |
| $C_{16}$ | - | 2.58 | 1.62 | 0.19 |
| $C_{17}$ | - | 2.53 | 1.59 | 0.19 |
| $C_{18}$ | - | 1.79 | 1.12 | 0.13 |
| $C_{19}$ | - | 2.19 | 1.37 | 0.16 |
| $C_{20}$ | - | 1.53 | 0.96 | 0.11 |
| $C_{21}$ | - | 1.43 | 0.89 | 0.10 |
| $C_{22}$ | - | 1.35 | 0.85 | 0.10 |
| $C_{23}$ | - | 1.24 | 0.78 | 0.10 |
| $C_{24}$ | - | 1.14 | 0.72 | 0.09 |
| $C_{25}$ | - | 1.07 | 0.67 | 0.08 |
| $C_{26}$ | - | 1.02 | 0.64 | 0.07 |
| $C_{27}$ | - | 0.66 | 0.41 | 0.05 |
| $C_{28}$ | - | 0.93 | 0.59 | 0.07 |
| $C_{29}$ | - | 0.62 | 0.39 | 0.04 |
| $C_{30}$ | - | 0.60 | 0.38 | 0.04 |
| $C_{31}$ | - | 0.59 | 0.37 | 0.04 |
| $C_{32}$ | - | 0.82 | 0.51 | 0.06 |
| $C_{33}$ | - | 0.45 | 0.28 | 0.04 |
| $C_{34}$ | - | 0.41 | 0.26 | 0.03 |
| $C_{35}$ | - | 0.52 | 0.33 | 0.04 |
| $C_{36}$ | - | 0.29 | 0.19 | 0.02 |
| $C_{37+}$ | - | 10.92 | 6.86 | 0.84 |
| | 100.00 | 100.01 | 99.99 | 99.97 |

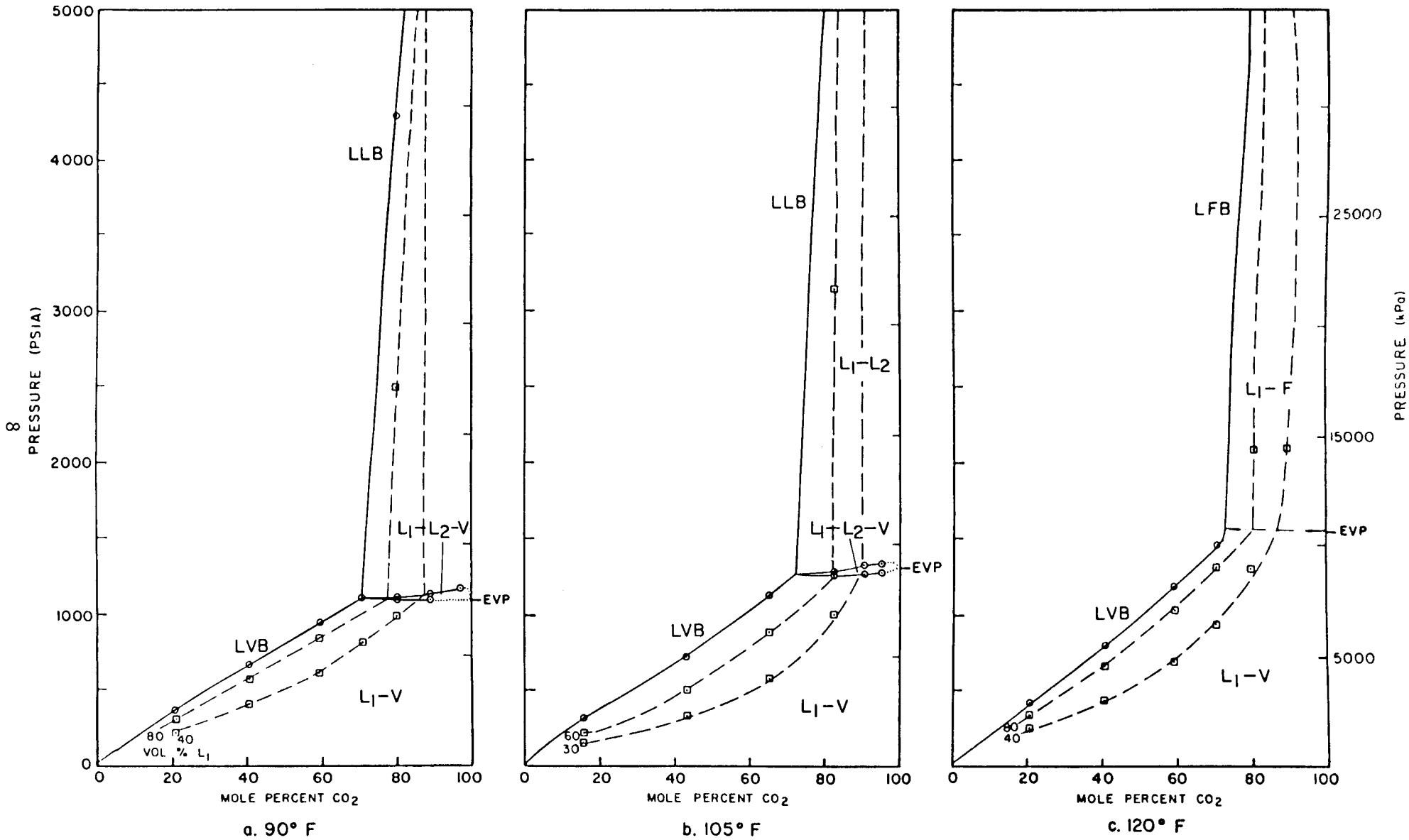


Fig. 2.1 Pressure-composition phase diagrams for mixtures of $CO_2$ with Wasson oil.

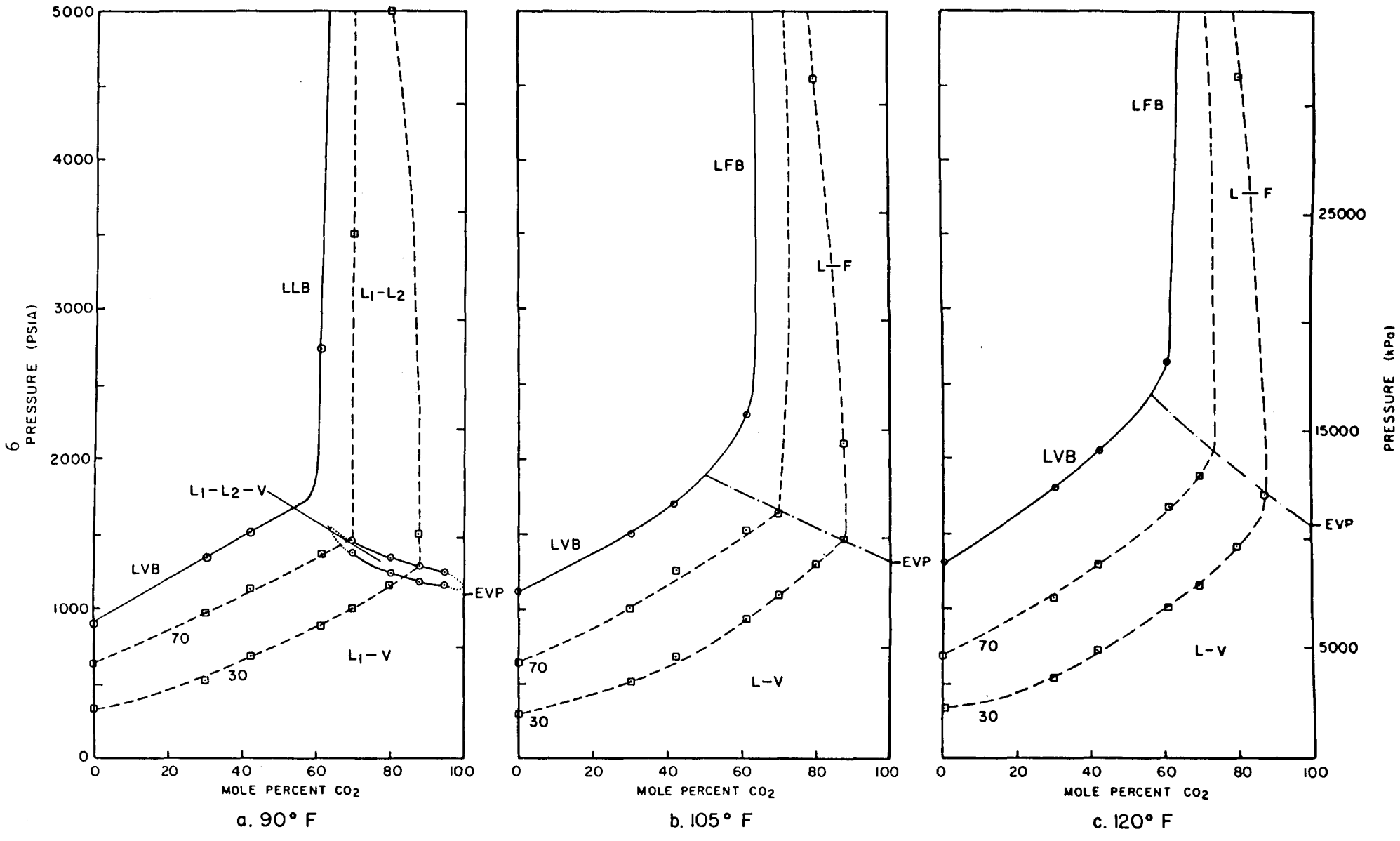


Fig. 2.2 Pressure-composition phase diagrams for mixtures of $CO_2$ with a recombined Wasson oil containing 312 SCF/BBL.

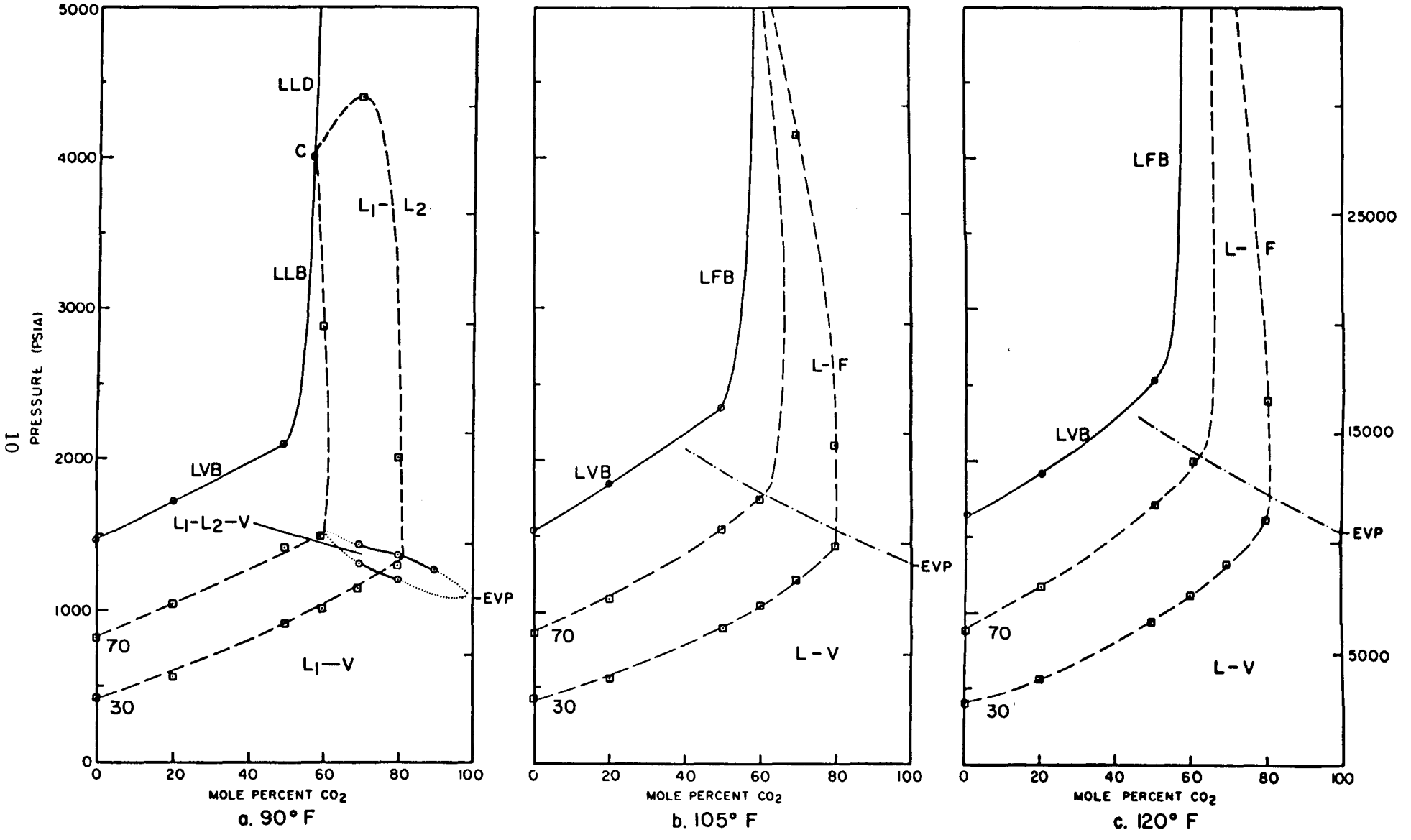


Fig. 2.3 Pressure-composition phase diagrams for mixtures of $CO_2$ with a recombined Wasson oil containing 602 SCF/BBL.

Much of the material in this section is also available in a paper by Orr and Jensen (1984). In that paper the behavior of two well characterized ternary systems, $CO_2$-$C_1$-$C_{16}$ and $CO_2$-$C_3$-$C_{16}$ is reviewed. Based on an analysis of P-X diagrams for the simpler hydrocarbon systems, Orr and Jensen concluded that liquid-liquid and liquid-liquid-vapor behavior in $CO_2$-crude oil systems is qualitatively very similar to that observed in well-characterized systems. Thus, the complex behavior of $CO_2$-crude oil systems at temperatures near the critical point of $CO_2$ (31°C) can be interpreted in terms of the behavior of well-characterized $CO_2$-hydrocarbon systems. Additional experimental details are given in the paper, and complete volumetric data for the experiments are also available (Jensen & Orr 1982a,b,c).

In Fig. 2.1, the phase behavior of mixtures of $CO_2$ with the dead oil alone is compared. At 90°F, liquid-vapor bubble points (LVB) were observed for $CO_2$ concentrations up to about 70 mol %. At higher $CO_2$ concentrations, a three-phase ($L_1$-$L_2$-V) region appeared. At high pressures and high $CO_2$ concentrations, two liquid phases were present in the cell. The only phase transition observed in the $L_1$-$L_2$ region was a liquid-liquid bubble point (LLB). Hence, no critical point is shown in Fig. 2.1a. Similar behavior was observed at 105°F, as shown in Fig. 2.1b. The L-V bubble point pressure curve shifted upward as additional pressure was required to force the more volatile $CO_2$ into solution in the oil. In addition, the three-phase region also shifted to higher pressures. At 120°F, Fig. 2.1c, the bubble point curve shifted to still higher pressures, and the $L_1$-$L_2$-V region disappeared. One mixture, containing 80.1 mol % $CO_2$, was investigated at 115°F (46°C). That mixture did form three phases. Thus, it appears that the maximum temperature for the formation of three phases was between 115 and 120°F for this oil. In Fig. 2.1c, the upper phase at high $CO_2$ concentrations and high pressures is a dense supercritical phase (F). The L-F bubble point pressures (LFB) increased sharply when the $CO_2$ concentration reached about 70 mol %.

Also shown in Fig. 2.1 are contours of constant volume fraction of the oil-rich ($L_1$) phase, normally the lowest in the cell. For one mixture containing 89.5 percent $CO_2$, however, a phase inversion was observed at 90°F. At pressures above 5800 psia (40,000 kPa), the $CO_2$-rich ($L_2$) liquid phase, dark orange in color, appeared at the bottom of the cell with the black $L_1$ phase at the top. Below 5800 psia the $L_2$ phase was on top. The approximate locations of the volume fraction contours are obtained from a plot of the fraction of the total cell volume occupied by the $L_1$ phase, an example of which is shown in Fig. 2.4. The locations of the contours in the $L_1$-V region are well-defined, but are less so in the $L_1$-$L_2$ region above about 1100 psia (7580 kPa), because the volumes of the two liquid phases are much less sensitive to changes in pressure. Thus, the contours are nearly vertical in the $L_1$-$L_2$ region. At 120°F (Fig. 2.1c), the contours climb very steeply at high $CO_2$ concentrations and high pressures even though the sharp distinction between $L_1$-$L_2$, $L_1$-V separations has disappeared. The pressure at which the volume fraction contours climb steeply (easily identified from plots like Fig. 2.1) indicates the pressure required to force the $CO_2$-rich $L_2$ phase to be a dense, relatively incompressible phase. The locus of pressures at which the $L_2$ phase became less compressible is shown as an almost horizontal dashed line in Fig. 2.1c.

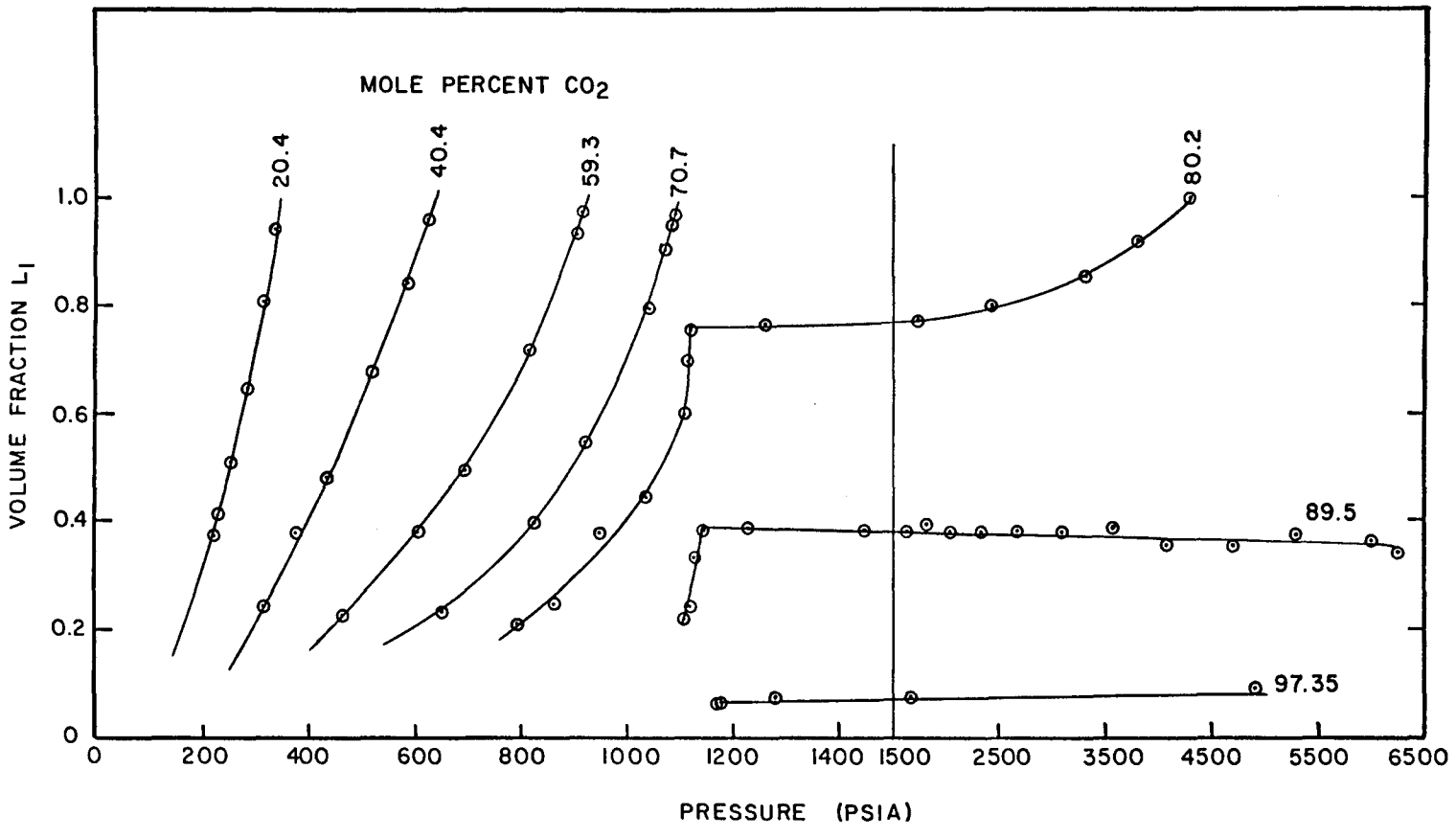


Fig. 2.4 Typical phase volume data for mixtures of $CO_2$ with Wasson oil at 90°F (32°C).

P-X diagrams for mixtures of $CO_2$ with a recombined oil containing 312 SFC/BBL are shown in Fig. 2.2. At all three temperatures, the multiphase region was significantly larger than it was for the dead oil. Only at 90°F did an $L_1$-$L_2$-V region appear. The $L_1$-$L_2$-V region sloped to lower pressures with increasing $CO_2$ concentration, and hence, the behavior of this system was similar to that described by Orr and Jensen (1984) for the $CO_2$-$C_1$-$C_{16}$ system. At 90°F, the $L_1$-$L_2$-V region was clearly separated from the bubble point curve. A mixture containing 61.5 mol % $CO_2$ exhibited a liquid-dense phase bubble point at 2750 psia (18960 kPa) but did not form three phases at any lower pressure. Mixtures containing 69.9, 80.0, 87.8 and 95.0 mol % $CO_2$, however, did form three phases.

At 105 and 120°F, no three-phase region was observed. Evidently, the addition of gas to an oil reduces the maximum temperature at which three phases can form. In both cases, mixtures containing more than about 60 mol % $CO_2$ changed from an oil-rich liquid in equilibrium with a dense $CO_2$-rich liquid (F) at very high pressures to a liquid and a vapor at low pressures, but without the appearance of a second interface. The saturation pressures observed at 105 and 120°F at 60 mol % $CO_2$ were bubble point pressures at which the dense $CO_2$-rich phase appeared at the top of the cell as the pressure was reduced. Saturation pressures of this type are labeled LFB in Figs. 2.1, 2.2 and 2.3.

At all three temperatures, contours of constant volume fraction $L_1$ climbed steeply at high $CO_2$ concentrations and high pressures. The loci of pressures and compositions at which the compressibility of the two-phase mixture dropped sharply are indicated in Fig. 2.2b and c.

Fig. 2.3 gives results of the phase behavior experiments for the recombined oil containing 602 SFC/BBL. Only at 90°F was a three-phase region observed. In addition, there was volumetric evidence for a critical point in the neighborhood of 60 mol % $CO_2$ and 4000 psia (27,000 kPa). The exact location of the critical point was not determined. In all the $CO_2$-oil mixtures studied in this set of experiments, phase transitions at pressures above about 4000 psia (20,700 kPa) were very difficult to observe because the two dense phases present had only slightly different densities and therefore separated very slowly. In addition, some mixtures separated into two phases if left long enough, but both phases were so dark in color that it was difficult to measure phase volumes. Thus, in all the phase diagrams shown here, the high pressure portions of the diagrams are less precisely known than the portions at low pressures. The locations of the three-phase regions were easily determined, however.

## Estimation of MMP: Effect of Temperature

In the ternary systems described by Orr and Jensen (1984), the $L_1$-$L_2$-V region on the P-X diagram always occurs at pressures near the three-phase pressure for mixtures of $CO_2$ with the heavy hydrocarbon component. That pressure is, in turn, close to the vapor pressure of $CO_2$, extrapolated if necessary for temperatures above that critical to $CO_2$. Fig. 2.5 shows how close the three-phase pressure is to the vapor pressure of $CO_2$ for $CO_2$-$C_{16}$

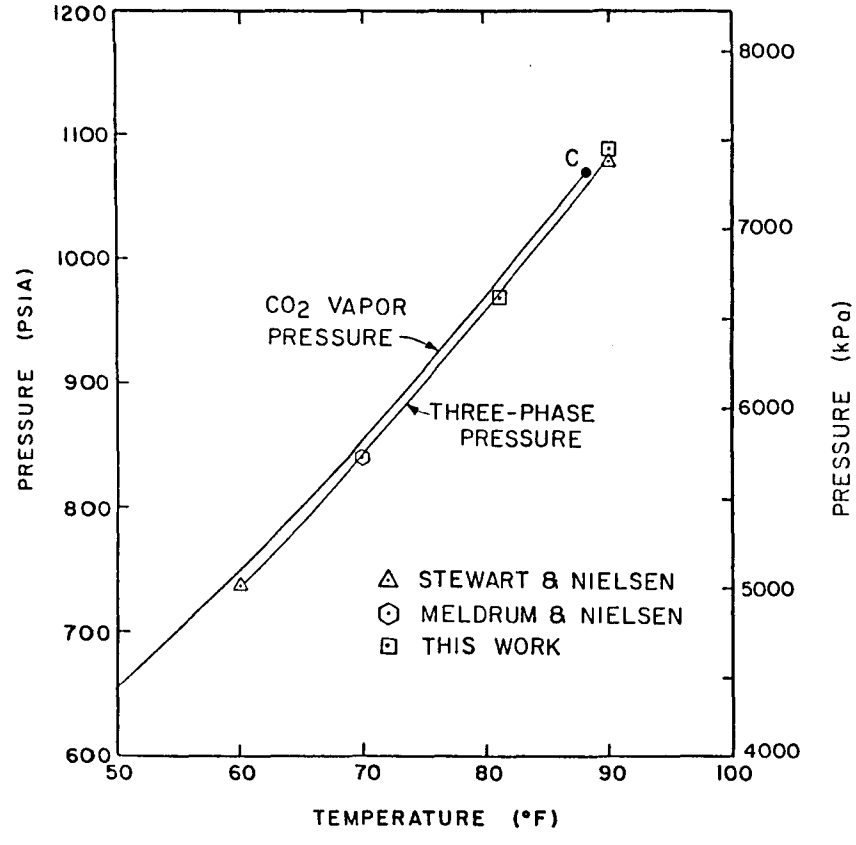


Fig. 2.5 Comparison of three-phase pressures for $CO_2$-hexadecane mixtures with the vapor pressure of $CO_2$.

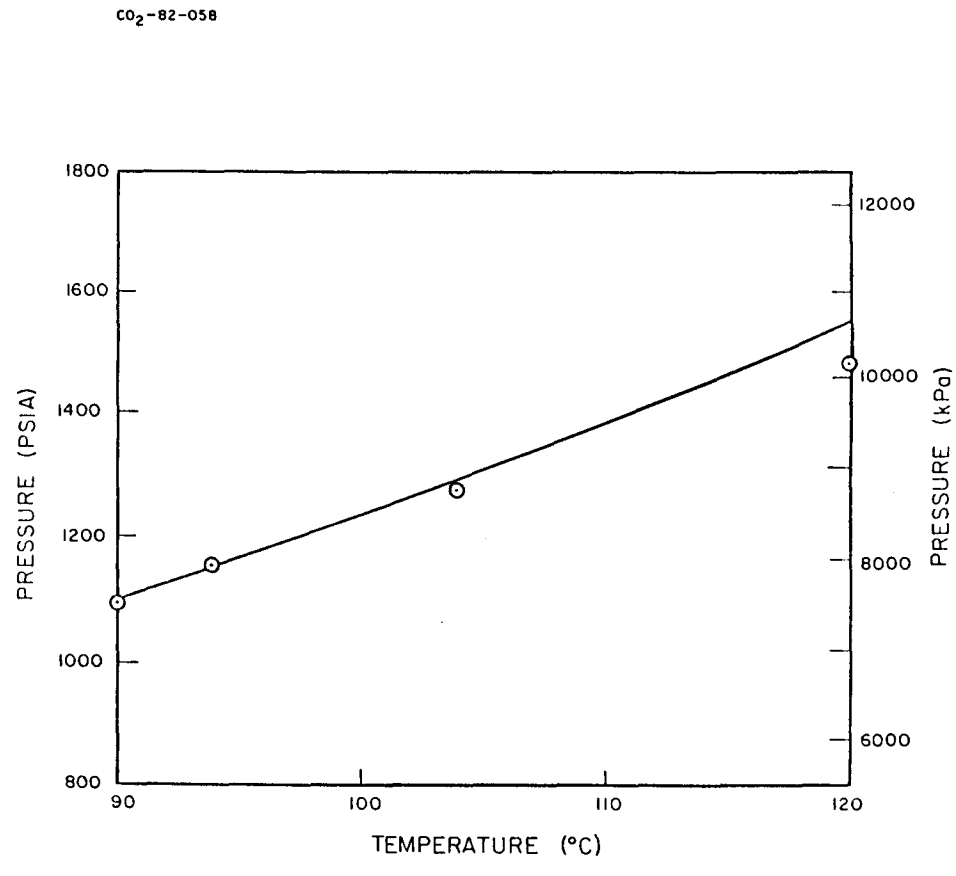


Fig. 2.6 Comparison of the extrapolated vapor pressure of $CO_2$ (solid line) calculated with eq. (2.1) with the pressure required to give a $CO_2$ density of 0.42 g/cm$^3$.

mixtures. Thus, the extrapolated vapor pressure (EVP) of $CO_2$ is a good estimate of the pressure near which $L_1$-$L_2$-V behavior will be observed if it occurs (Orr, Lien & Pelletier 1981). A convenient equation for the vapor pressure of $CO_2$ has been given by Newitt et al (1956)

$$P = 101.3 \exp\left\{\frac{-2015}{T} + 10.91\right\} \qquad (2.1)$$

where P is the vapor pressure in kPa, and T the temperature in °K.

It is clear from Figs. 2.1-2.3 in which the extrapolated vapor pressure is labeled EVP, that the crude oil systems investigated here all show $L_1$-$L_2$-V separations at pressures near the extrapolated vapor pressure, if they show such behavior at all. The extrapolated vapor pressure is also a good estimate of the pressure required to make the $CO_2$-rich phase dense enough to be relatively incompressible. In the dead oil system, the $CO_2$-rich phase at 120°F behaves much like the $L_2$ phases at 90 and 105°F when the pressure is above the EVP, as comparison of Fig. 2.1c with Fig. 2.1a and b indicates. In the recombined oil systems, the curves which mark the pressures at which the overall compressibility changes sharply all appear to terminate at the EVP. This behavior is not surprising since the EVP correlation provides a good estimate of the location in pressure of the steep portion of the $CO_2$ density curve, at least for the temperature range investigated here (Michels, Botzen & Schuurman 1957).

Estimates of the pressure required to produce a dense $CO_2$-rich phase are of more than academic interest. It has been shown that a dense $CO_2$-rich liquid extracts hydrocarbons more efficiently than a $CO_2$-rich vapor phase at the same pressure (Orr, Silva & Lien 1983). In addition, Holm and Josendal (1982) have argued that the principal effect of changing system temperature is to change the pressure required to make the $CO_2$ dense enough to extract hydrocarbons efficiently. They argued that the minimum density required was about 0.42 $g/cm^3$, though heavier oils required higher $CO_2$ densities. Fig. 2.6 compares the EVP correlation given as eq. (2.1) with the pressure required to give a $CO_2$ density of 0.42. It is clear that the EVP curve gives a good estimate, particularly if the temperature is at a lower end of the range.

We have shown here that the extrapolated vapor pressure is a good estimate of the pressure above which $L_1$-$L_2$-V behavior will be observed if it occurs, and that it also provides an indication of the pressure required to make the $CO_2$-rich phase behave as a dense, relatively incompressible phase. It is just such a phase that will extract hydrocarbons efficiently. That extraction will, in turn, lead to an efficient local displacement (Gardner, Orr & Patel 1981; Orr, Yu & Lien 1981; Orr, Silva & Lien 1983) such as would occur in a slim tube displacement at a pressure above the MMP. Thus, in the absence of other experimental evidence, the extrapolated vapor pressure curve can be used as an estimate of the MMP. This estimate is likely to be accurate for dead oils, but may be less so if the oil contains substantial quantities of dissolved gas. Figs. 2.1-2.3 clearly show that the pressure required to produce a relatively incompressible $CO_2$-rich phase depends on the mixture composition when gas is present, though it is clear that at high $CO_2$

concentrations, the limiting value of the pressure required is the EVP. It is possible that a $CO_2$ displacement could still be efficient even if some portion of the process passes through a region where the density of the $CO_2$-rich phase is low as long as a dense $CO_2$-rich phase is created eventually. This idea has not been tested experimentally, however.

A comparison of the extrapolated vapor pressure estimate of the MMP with measured values reported by a variety of investigators is given in Fig. 2.7. For temperatures below about 140°F, the agreement is excellent, though with a few exceptions. Some of those, however, were systems in which the investigators did not test pressures below the bubble point. Instead, the bubble point was taken as the MMP, as suggested by Yellig and Metcalfe (1980) and Holm and Josendal (1982). Thus, it is not known whether high recoveries would have resulted at lower pressures. The extrapolated vapor pressure curve is compared with the correlations offered by Yellig and Metcalfe (1980) and Holm and Josendal (1982) in Fig. 2.7. Again, the agreement is good. Thus, the MMP estimate offered here differs little from correlations previously available. It does, however, offer a clear physical explanation for the behavior of such correlations at low temperature. The restriction to low temperatures is, of course, important. At low temperatures, the density of the $CO_2$-rich phase climbs so steeply at the extrapolated vapor pressure that effects of oil composition are all but swamped. At higher temperatures where density changes with pressure are more gradual, oil composition would have a larger impact.

## $CO_2$-$N_2$-Wasson Oil Mixtures

In the previous discussion, the idea that density of the $CO_2$-rich phase controls extraction was used to construct a simple estimate of the pressure required for efficient extraction. To examine the effects of changing the density of the $CO_2$-rich phase, phase behavior experiments were performed for mixtures of dead Wasson oil with a gas mixture containing 90 mol % $CO_2$ and 10 mol % $N_2$. As in the previous study, experiments were performed at 90, 105 and 120°F. Results of those measurements are summarized in Fig. 2.8. Comparison of Figs. 2.8 and 2.1 yields the following observations:

- Addition of $N_2$ increased substantially the size of the multiphase region. This corresponds to a decrease in the solubility of the gas in the oil.

- The $L_1$-$L_2$-V region disappeared at a lower temperature when $N_2$ was present.

- The pressure required to make the $CO_2$-rich phase a dense, relatively incompressible phase was a strong function of overall mixture composition and was higher when $N_2$ was present.

Also shown in Fig. 2.8 are the extrapolated vapor pressures at the three temperatures as well as the pressures at which the densities of the $CO_2$-$N_2$ mixture equal the critical density of $CO_2$, 0.42 g/cm$^3$ (labeled CDP in Fig. 2.8). Those pressures were calculated with a computer program (TRAPP), based

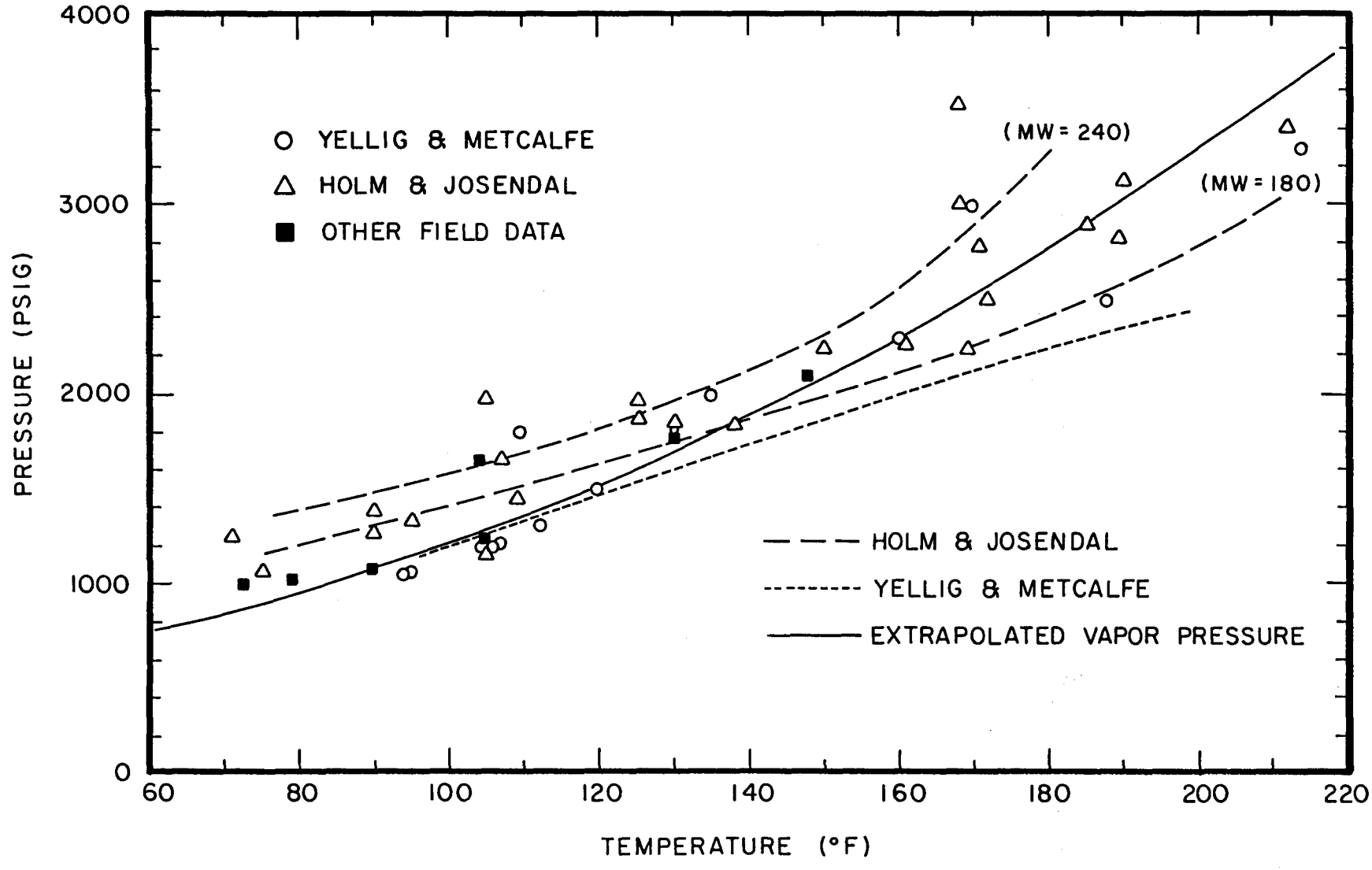


Fig. 2.7 Comparison of extrapolated vapor pressure with measured MMPs and MMP correlations (Yellig & Metcalfe 1980; Holm & Josendal 1982).

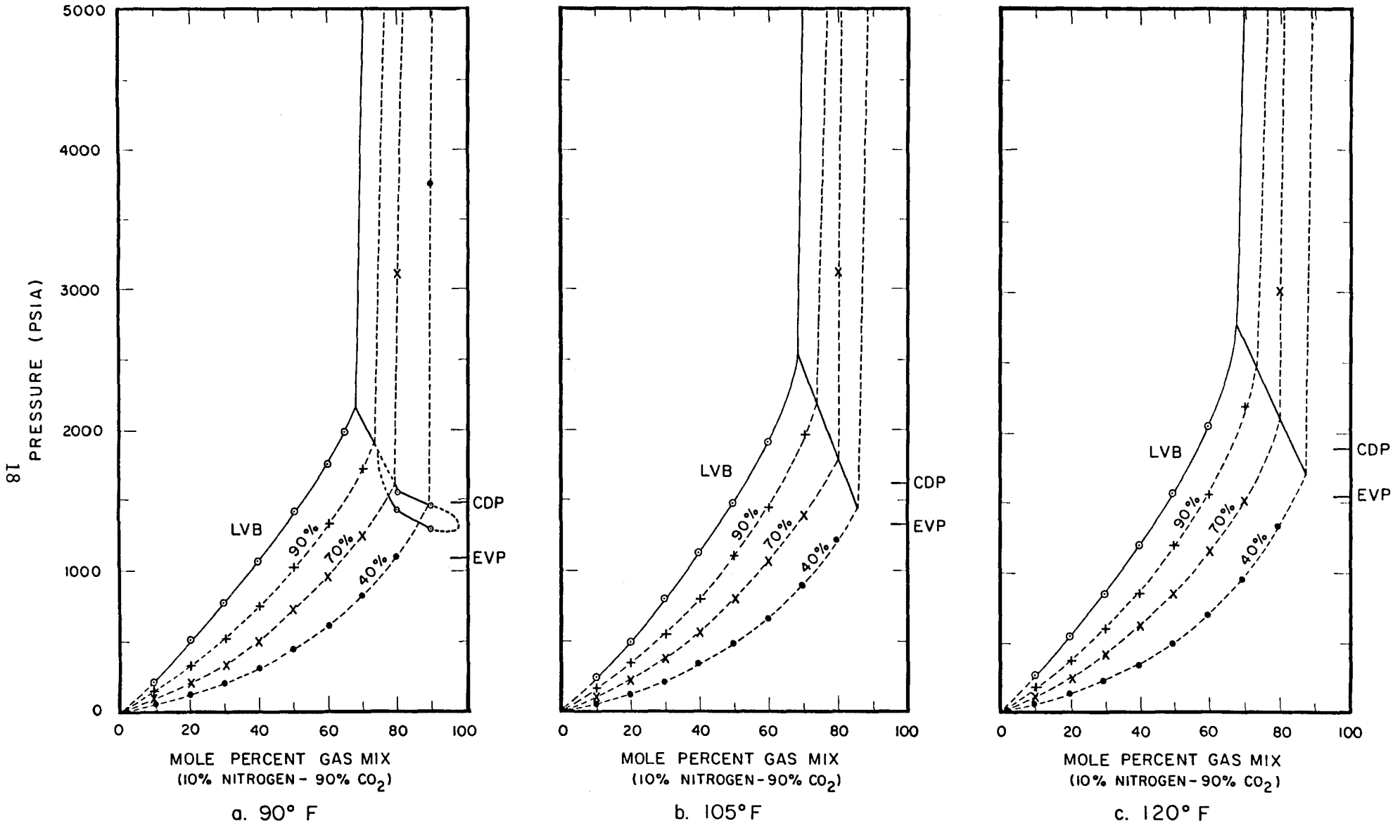


Fig. 2.8 Pressure-composition phase diagrams for mixtures of Wasson oil with $CO_2$ containing 10 mol % $N_2$.

on an extended corresponding states approach, written by Ely and Hanley (1981). It is clear from Fig. 2.8 that the CDP is a good estimate of the pressure at which three phases appear (Fig. 2.8a) at 90°F. At the higher temperatures, the CDP still gives a reasonable estimate of the pressure required to make the upper phase relatively incompressible if the gas concentration is high. At lower gas concentrations, the pressure required is significantly higher. One explanation for the dependence of that pressure on composition is that the $CO_2$ in the $CO_2$-$N_2$ mixture is more soluble in the oil than the $N_2$. Hence, the upper phase is richer in $N_2$ than the original $CO_2$-$N_2$ mixture. This effect must be greater when the gas concentration is lower because there is more oil present to be saturated with $CO_2$, and there is less gas present to supply the $CO_2$. The remaining $N_2$-rich upper phase must be compressed to a higher pressure to produce a dense, liquid-like phase.

## Estimation of MMP: Effect of Contamination of $CO_2$

The phase diagrams shown for the $CO_2$-$N_2$ system suggest that the shift in the location of the three-phase region and the pressure required to produce a dense, relatively incompressible upper phase is related to the reduction of the density of $CO_2$ by the $N_2$. The idea that the density of the injected fluid is important is the basis for the simple (EVP) correlation for MMPs given above and for the correlation given by Holm and Josendal (1982). They argued that the MMP must depend not only on the temperature but also on the composition of the oil being tested. They suggested that for a given oil, there is a specific density of $CO_2$ required to produce sufficient extraction of hydrocarbons from the oil into the $CO_2$-rich phase. They also argued that the density required depends on the composition of the oil. Oils rich in hydrocarbon components lighter than $C_{30}$, which are extracted more efficiently by $CO_2$ than are heavier hydrocarbons, apparently require a lower $CO_2$ density than do heavier oils.

The idea that there is some characteristic density of injected fluid at which sufficient extraction occurs is a useful simplification, even though it clearly does not reflect the full detail of the phase behavior of the very complex chemical mixtures. For instance, if the required density were determined for an oil with an injection gas at a given temperature, the effect of changes in temperature or gas composition could be estimated easily by calculating the pressure required to reach the same density at the new conditions. Experimentally determined MMPs reported by Metcalfe (1982) were used to test this procedure. Metcalfe investigated the effect of the addition of contaminants such as methane, hydrogen sulfide ($H_2S$), ethane ($C_2$), propane ($C_3$), and butane ($C_4$) on MMPs for $CO_2$ displacements of two oils at several temperatures. For each of the oils, the density of the injected gas at the highest reported MMP was used as an estimate of the required density. The highest MMP was used because there was less uncertainty in the density for the systems at the highest temperature and pressure, as is illustrated in Fig. 2.9 which reports $CO_2$ density at the MMP for one of the systems studied by Metcalfe. The uncertainty arises from the fact that the slim tube displacements are run with typical pressure increments of at least 100 psia. Thus, the MMP is determined only to the resolution of the pressure increment. At low temperatures, a small change in pressure can lead to a large difference

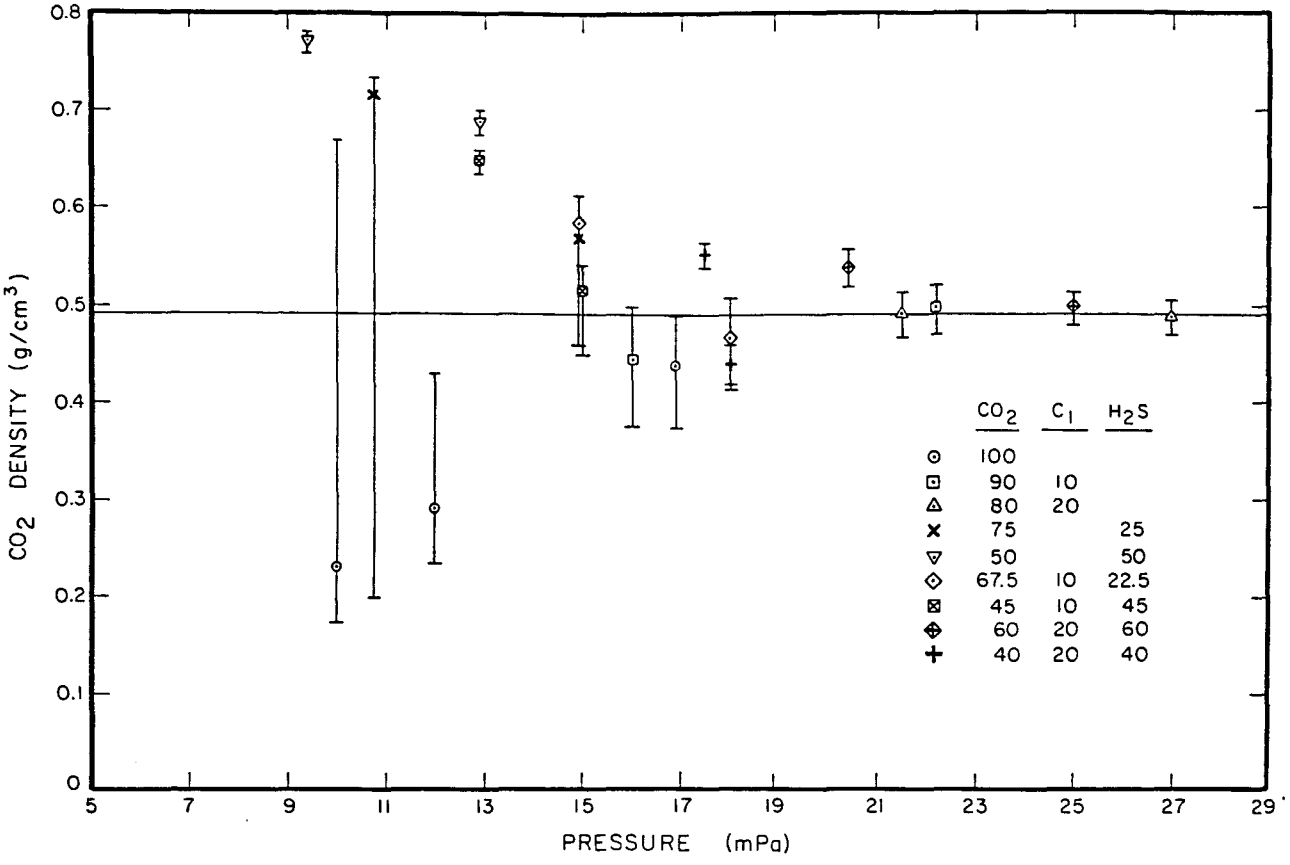


Fig. 2.9 Injected fluid density at the MMP. MMPs were measured by Metcalfe (1982). Error bars indicate density at the MMP ±100 psia. Densities were calculated with TRAPP (Ely & Hanley 1981).

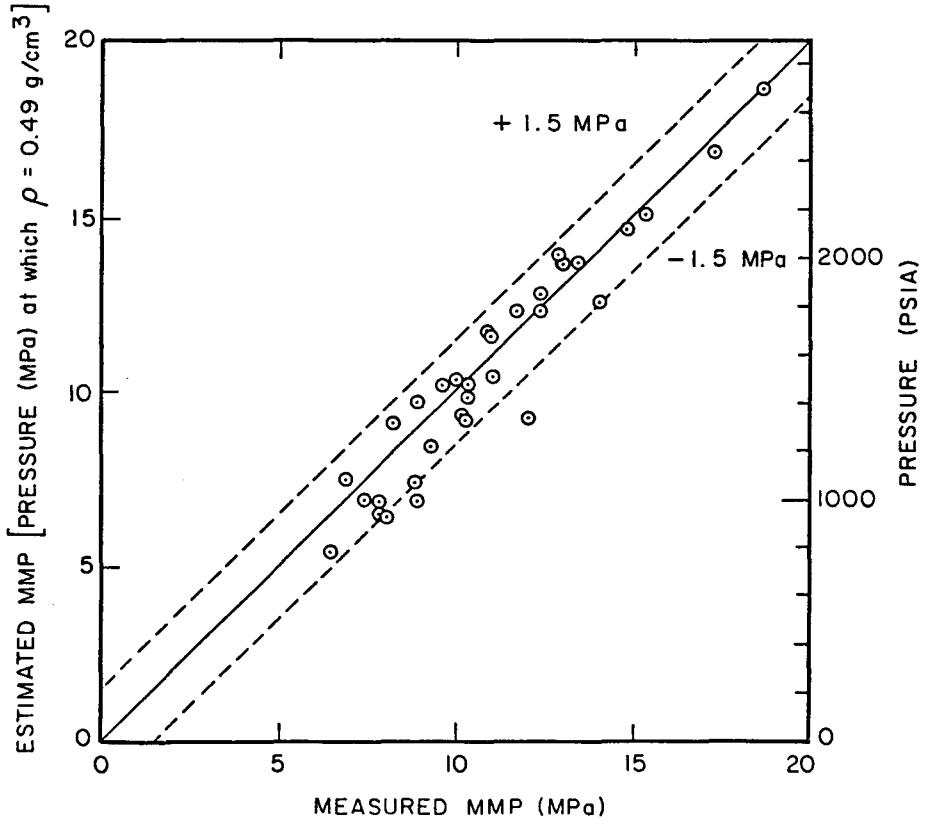


Fig. 2.10 Comparison of estimated and measured MMPs (Metcalfe 1982) for two west Texas oils at a variety of temperatures.

in density as is shown by the error bars corresponding to the densities of $CO_2$ at 100 psi above and below the reported MMP. Hence, the density at the MMP is determined less accurately at low temperature. For both oils, the injected fluid had a density of about 0.49 g/cm$^3$ at the highest MMP. MMPs for all of the other injected gas mixtures and temperatures were then predicted as the pressure required to produce a gas density of 0.49 g/cm$^3$. Densities of the injected mixtures were all calculated with TRAPP (Ely & Hanley 1981). Results of the predictions are compared with the measured MMPs in Table 2.2 and Fig. 2.10.

The agreement shown in Fig. 2.10 suggests that the effects of the addition of contaminants to $CO_2$ or other miscible gas or of changes in temperature can be estimated easily if at least some MMP data are available. For instance, for the oils examined by Metcalfe, the estimated effects of the addition of methane or nitrogen to $CO_2$ are shown in Figs. 2.11 and 2.12. Contamination of the $CO_2$ by either $C_1$ or $N_2$ raises the MMP appreciably. At low temperatures, $N_2$ has a larger effect. At high temperatures, there is little difference between $C_1$ and $N_2$.

One additional test of the estimation procedure was performed. MMPs for two oils reported by Johnson and Pollin (1981) for mixtures of $CO_2$ and $N_2$ were estimated. Table 2.3 and Fig. 2.13 compare the measured MMPs with the estimated values. Again, the agreement is reasonable. It appears, therefore, that the effects of contamination and temperature changes on the MMP can be estimated with an accuracy of about ±1.5 MPa as long as the density required for the particular oil is known or can be estimated. This sort of procedure should be used with care, however, if the changes in composition or temperature are large. For instance, Stalkup (1983) reports a correlation for MMPs for methane displacements. Calculated densities of $C_1$ at the measured MMPs for the nine oils for which Stalkup gives experimental results (see Table 2.4) were all close to 0.15 g/cm$^3$, much lower than the 0.4 to 0.5 g/cm$^3$ typical of $CO_2$ systems, though the difference in molar densities was smaller, 9.4 moles/ℓ for $C_1$ vs. 9.1 to 11.4 moles/ℓ for $CO_2$. Estimates of MMPs based on the assumption of constant molar density did not agree as well with Metcalfe's measured values, however. Clearly, there is room for additional research to improve predictions of the conditions required to produce multiple contact miscibility.

## 2.2 Component Partitioning in $CO_2$-Hydrocarbon Systems

The importance of extraction of hydrocarbons by $CO_2$ in the generation of high microscopic displacement efficiency is by now well established. The simple correlation for MMP discussed above and the more general correlation offered by Holm and Josendal (1982) both are based on the idea that density of $CO_2$ controls extraction. It must also be true, however, that the efficiency with which different hydrocarbons are extracted depends, to some extent at least, on the size and type of the hydrocarbon molecules. For instance, Holm and Josendal made use of the idea that hydrocarbons in the $C_5$-$C_{30}$ range are extracted more efficiently than heavier ones in the formulation of their MMP

Table 2.2 Comparison of Measured and Estimated Minimum Miscibility Pressures

Oil A

| $CO_2$ | $C_1$ | $H_2S$ | T | Measured MMP | Estimated MMP |
|---|---|---|---|---|---|
| (Mole Percent) | | | (°K) | (MPa) | (MPa) |
| 100 | -- | -- | 305 | 6.9 | 7.5 |
| 100 | -- | -- | 314.8 | 8.3 | 9.1 |
| 100 | -- | -- | 331.5 | 11.7 | 12.3 |
| 90 | 10 | -- | 314.8 | 11.0 | 11.6 |
| 90 | 10 | -- | 331.5 | 15.3 | 15.0 |
| 80 | 20 | -- | 314.8 | 14.8 | 14.6 |
| 80 | 20 | -- | 331.5 | 18.6 | 18.6 |
| 75 | -- | 25 | 314.8 | 7.4 | 6.9 |
| 75 | -- | 25 | 331.5 | 10.2 | 9.3 |
| 50 | -- | 50 | 314.8 | 6.5 | 5.4 |
| 50 | -- | 50 | 331.5 | 8.9 | 7.4 |
| 67.5 | 10 | 22.5 | 314.8 | 10.3 | 9.2 |
| 67.5 | 10 | 22.5 | 331.5 | 12.4 | 12.8 |
| 45 | 10 | 45 | 314.8 | 8.9 | 6.9 |
| 45 | 10 | 45 | 331.5 | 10.3 | 10.2 |
| 60 | 20 | 20 | 314.8 | 14.1 | 12.5 |
| 60 | 20 | 20 | 331.5 | 17.2 | 16.8 |
| 40 | 20 | 40 | 314.8 | 12.1 | 9.2 |
| 40 | 20 | 40 | 331.5 | 12.4 | 12.3 |

Oil B

| $CO_2$ | $C_2$ | $C_3$ | $C_4$ | T | Measured MMP | Estimated MMP |
|---|---|---|---|---|---|---|
| (Mole Percent) | | | | (°K) | (MPa) | (MPa) |
| 100 | -- | -- | -- | 322 | 11.0 | 10.4 |
| 100 | -- | -- | -- | 339 | 13.4 | 13.7 |
| 90 | 10 | -- | -- | 322 | 10.0 | 10.3 |
| 90 | 10 | -- | -- | 339 | 13.0 | 13.7 |
| 80 | 20 | -- | -- | 322 | 9.7 | 10.2 |
| 80 | 20 | -- | -- | 339 | 12.9 | 13.9 |
| 90 | -- | 10 | -- | 322 | 9.3 | 8.4 |
| 90 | -- | 10 | -- | 339 | 11.0 | 11.7 |
| 80 | -- | 20 | -- | 322 | 7.9 | 6.6 |
| 80 | -- | 20 | -- | 339 | 10.3 | 9.9 |
| 90 | -- | -- | 10 | 322 | 7.9 | 6.8 |
| 90 | -- | -- | 10 | 339 | 9.0 | 9.7 |
| 80 | -- | -- | 20 | 339 | 8.1 | 6.4 |

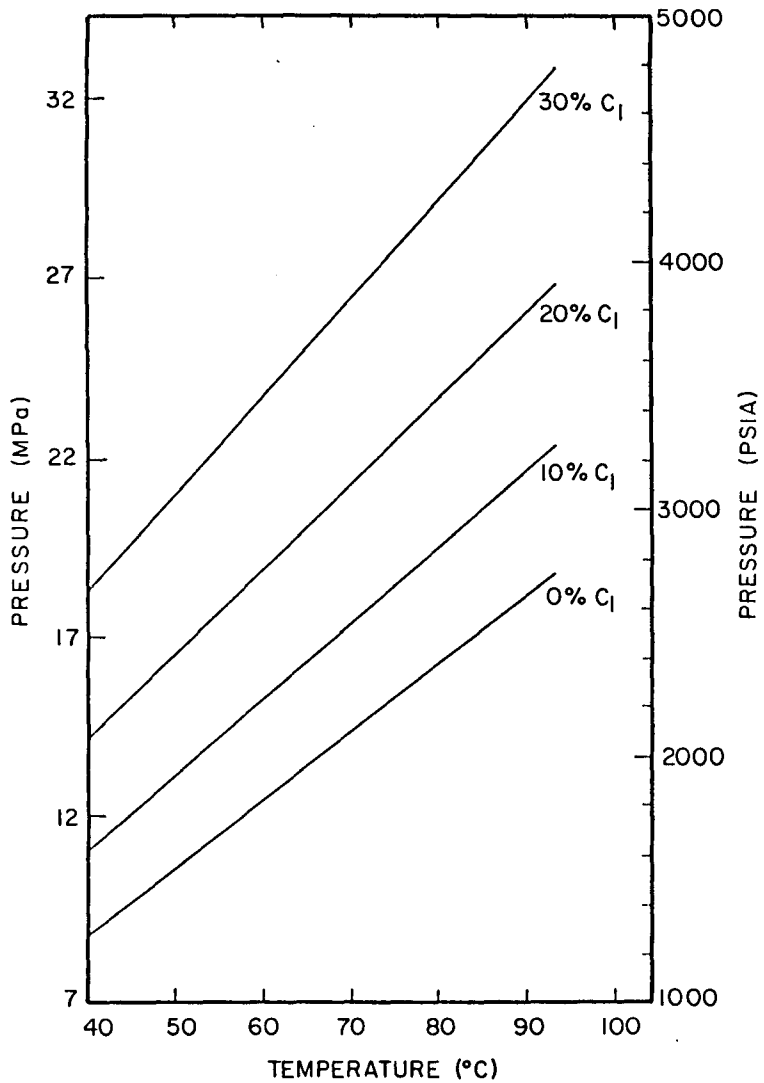


Fig. 2.11 Estimated MMPs for displacement of a Permian basin oil by $CO_2$ contaminated with methane.

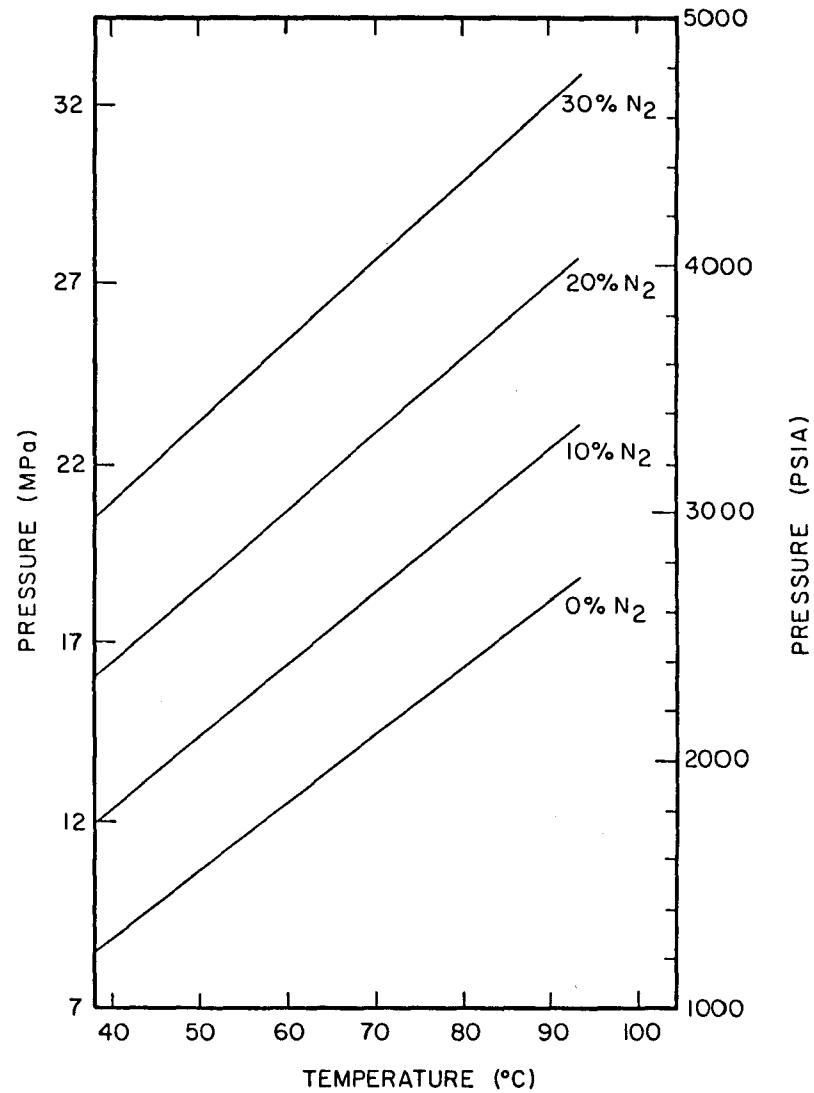


Fig. 2.12 Estimated MMPs for displacement of a Permian basin oil by $CO_2$ contaminated with nitrogen.

Table 2.3 Comparison of Measured and Estimated Minimum Miscibility Pressures

Oil A

| $CO_2$ | $N_2$ | $C_1$ | T | Measured MMP | Estimated MMP |
|---|---|---|---|---|---|
| (Mole Percent) | | | (°K) | (MPa) | (MPa) |
| 100 | -- | -- | 330 | 11.3 | 13.2 |
| 97 | 3 | -- | 330 | 13.0 | 14.7 |
| 94 | 6 | -- | 330 | 15.5 | 16.2 |
| 90 | 10 | -- | 330 | 18.4 | 18.4 |

Oil D

| $CO_2$ | $N_2$ | $C_1$ | T | Measured MMP | Estimated MMP |
|---|---|---|---|---|---|
| (Mole Percent) | | | (°K) | (MPa) | (MPa) |
| 100 | -- | -- | 301 | 6.9 | 7.0 |
| 94 | 6 | -- | 301 | 12.4 | 12.1 |
| 89 | 11 | -- | 301 | 16.7 | 16.8 |
| 86 | 14 | -- | 301 | 19.8 | 19.8 |
| 94 | -- | 6 | 301 | 8.6 | 10.9 |

Table 2.4 Calculated Density of Methane at Measured Minimum Miscibility Pressures for Vaporizing Gas Drives

| Oil | T (°K) | MMP (MPa) | Density at MMP ($g/cm^3$) |
|---|---|---|---|
| 1 | 333 | 22.8 | 0.146 |
| 2 | 402 | 32.7 | 0.150 |
| 3 | 390 | 37.8 | 0.174 |
| 4 | 353 | 22.3 | 0.130 |
| 5 | 390 | 31.6 | 0.152 |
| 6 | 334 | 27.8 | 0.171 |
| 7 | 334 | 30.6 | 0.183 |
| 8 | 394 | 32.6 | 0.154 |
| 9 | 373 | 32.0 | 0.163 |

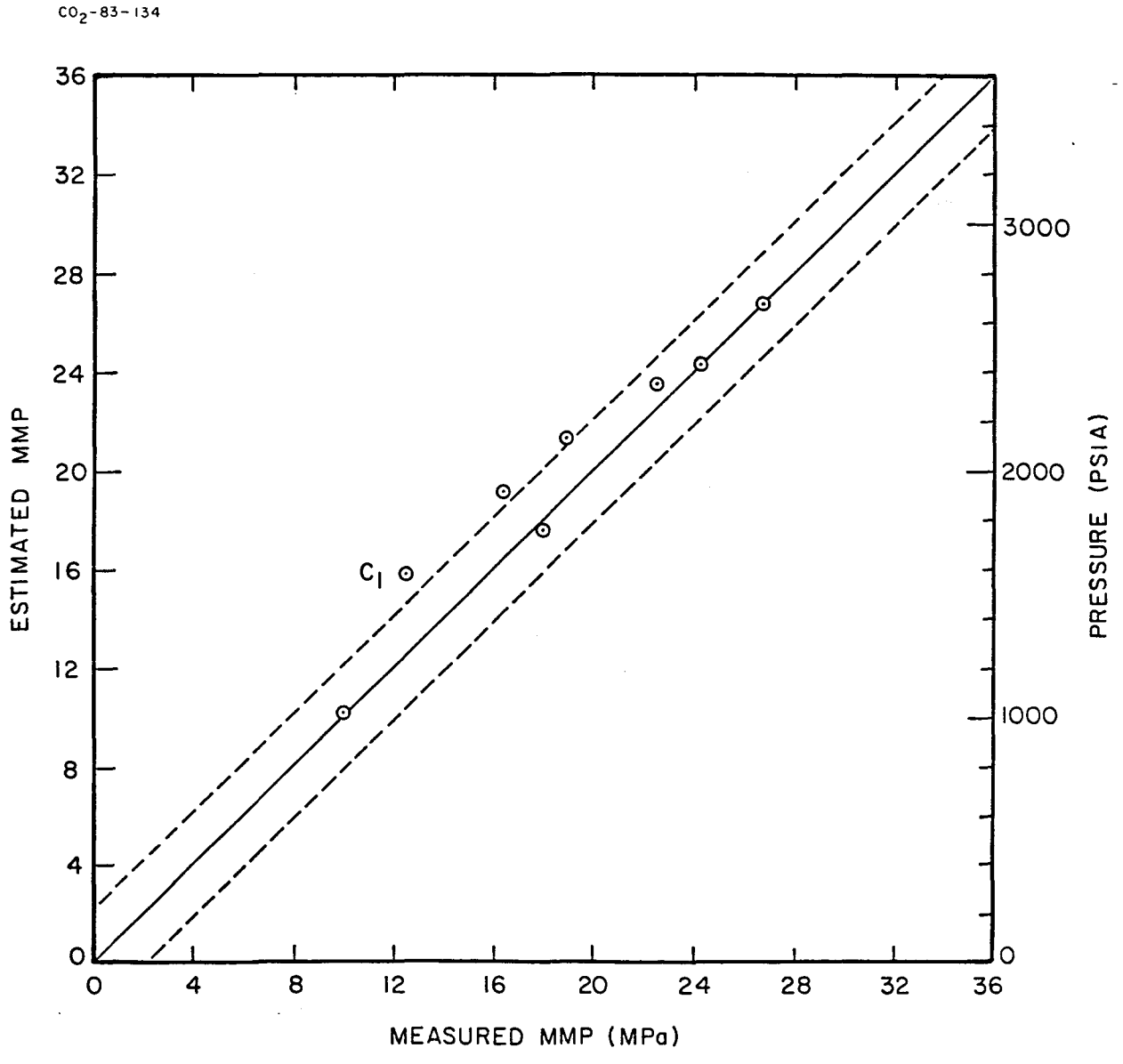


Fig. 2.13 Comparison of estimated and measured MMPs for two oils at two temperatures (Johnson & Pollin 1981). The injected fluid was $CO_2$ with varying amounts of nitrogen or methane added.

correlation. They also speculated that molecular type might influence extraction. In this section we report results of a sequence of experiments with crude and synthetic oils designed to investigate how oil composition, and hydrocarbon molecular type and size influence component partitioning in $CO_2$-hydrocarbon systems. Three questions are examined:

(1) To what extent does component partitioning depend on the nature of carbon-carbon (paraffinic, naphthenic, aromatic) bonds?

(2) How sensitive is extraction efficiency to the size of the molecules extracted?

(3) Does the distribution of hydrocarbon molecular weights present strongly affect amounts of heavy components extracted?

Phase compositions measured with the continuous multiple contact (CMC) apparatus are compared for three crude oil systems containing differing amounts of aromatics. Also compared are measurements of partitioning in four synthetic oil systems of similar overall molecular weight but composed of n-alkanes, branched alkanes, naphthenes and aromatics.

Also reported are detailed phase composition and density data for a quaternary system containing $CO_2$, $C_1$, $C_4$ and $C_{10}$. The measured results are compared with values computed with the Peng-Robinson equation of state. We also show that the Peng-Robinson equation produces good quantitative agreement between calculated and experimental phase compositions for mixtures of $CO_2$ with various hydrocarbons which show complex liquid-liquid and liquid-liquid-vapor separations.

## Experimental Procedure

Phase composition and density data reported below were obtained with the continuous multiple contact experiment. For clarity, a brief review of the technique is given here. More detailed descriptions of the apparatus, experimental procedure and results of experiments to validate the method are available elsewhere (Orr & Taber 1981; Orr & Silva 1983). Modifications to the apparatus which allow automatic control and data acquisition are described in Appendix A.

Unlike static equilibrium experiments which measure phase volumes for a constant composition mixture of $CO_2$ and hydrocarbons at various pressures, the CMC experiment produces samples from coexisting phases at constant pressure, but continuously changing overall composition. A schematic of the apparatus is shown in Fig. 2.14. A circulating pump mixes injected $CO_2$ with hydrocarbons initially charged into the cell. Quiescent zones at the top and bottom of the cell allow production of clean, equilibrated samples. The produced fluids flow through high pressure densitometers which, in addition to reporting density, signal the appearance of a second or even a third phase and verify that produced samples are not contaminated by another phase. Methods for determining upper and lower sample compositions are identical. After passing through a back pressure regulator, the fluids, which are now at

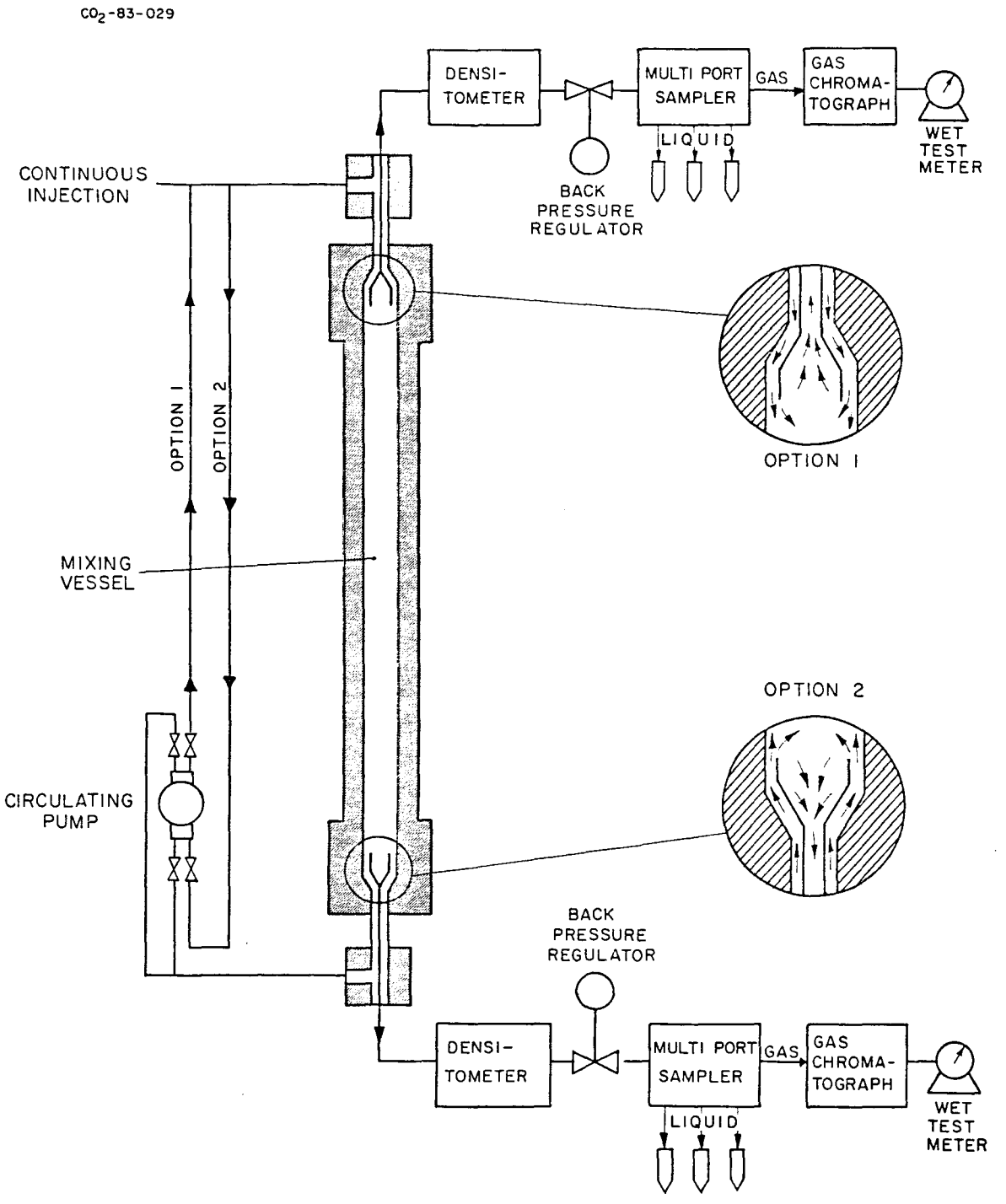


Fig. 2.14 Continuous multiple contact apparatus.

atmospheric pressure, usually split into two phases. The liquids, which generally contain $C_{5+}$ hydrocarbons, collect in sample vials for later weighing and compositional analysis by simulated distillation (Orr & Taber 1981). The separated vapor, composed of $CO_2$ and very volatile hydrocarbons, proceeds to a gas chromatograph for on-line compositional analysis and then to a wet test meter for measurement of volume. The amounts and compositions of both the liquid and gas collected during a sampling period are combined to calculate an overall composition for fluid produced during a certain time interval. Table 2.5, taken from a phase behavior study for a $CO_2$-crude oil system (Silva et al 1981a), illustrates the detail of compositional information available for each sample. In Fig. 2.15, results of that study are summarized in a pseudo-ternary phase diagram in which the oil is represented as two lumped components, $C_5$-$C_{12}$ and $C_{13+}$. Continuous injection of $CO_2$ causes the concentration of $CO_2$ to increase until the two-phase region is reached. Subsequent samples scan a sequence of tie lines in the two-phase region.

## $CO_2$-Crude Oil Systems

Figs. 2.16 and 2.17 give pseudo-ternary representations of the phase behavior of $CO_2$ mixed with separator crude oils from the Maljamar field, Lea County, New Mexico and the Rock Creek field, Roane County, West Virginia, respectively. Table 2.6 lists the properties of each system and the experimental conditions. Based on proton NMR measurements, the crude oil from the Maljamar field was estimated to contain approximately 8 wt. % aromatics and the highly paraffinic Rock Creek oil, less than 2 wt. % aromatics. The slopes of the tie lines and shapes of the two-phase envelopes of the two systems are similar, as shown in Figs. 2.16 and 2.17. Thus, the presence of the aromatics in the Maljamar crude oil had no obvious effect on component partitioning. A more detailed comparison of partitioning in the two systems is shown in Fig. 2.18, which reports equilibrium ratios for individual carbon number cuts. In each case, the K-values reported are for samples in the two-phase region that had about equal mole fractions of $CO_2$ in the upper phase. Again, there is little evidence of a substantial effect of the aromatics present in the Maljamar oil on component partitioning.

To examine further the role of aromatics in component partitioning, a continuous multiple contact experiment was performed for the Rock Creek oil to which a mixture of aromatics had been added. Table 2.7 gives the composition of the aromatic mixture added to the crude oil, and Table 2.8 reports the composition of the mixture. A more detailed discussion of sample preparation is given by Silva et al (1982a).

The phase diagram for the Rock Creek separator oil plus aromatics, presented in Fig. 2.19, showed a change in the shape of the phase envelope and the tie line slopes, though the magnitude of the change is not large. The two-phase region extended further toward the light hydrocarbon apex when aromatics were added. The change in the slopes of the tie lines is favorable, but it is at least partly compensated by the enlargement of the two-phase region, which displaces the critical tie line to higher concentrations of light hydrocarbons ($C_1$-$C_{12}$), an unfavorable change in the phase diagram (Orr, Jensen & Silva 1981).

Table 2.5 Compositions of Gas and Liquid Samples from CMC Experiment for Maljamar Crude Oil at 1400 psia and 90°F

LOWER PHASE SAMPLE 13

TOTAL WEIGHT OF OIL = 2.70 TOTAL WEIGHT OF GAS = 1.45 MOLE WEIGHT OF C37+ = 563.20

| | GAS ANALYSIS | | | | LIQUID ANALYSIS | | | | RECOMBINED DATA | | | |
|---|---|---|---|---|---|---|---|---|---|---|---|---|
| C# | WT FR | CUM | MOL FR | CUM | WT FR | CUM | MOL FR | CUM | WT FR | CUM | MOL FR | CUM |
| CO2 | 0.9090 | | 0.9455 | | 0.0000 | | 0.0000 | | 0.3175 | | 0.7033 | |
| 1 | 0.0000 | 0.0000 | 0.0000 | 0.0000 | 0.0000 | 0.0000 | 0.0000 | 0.0000 | 0.0000 | 0.0000 | 0.0000 | 0.0000 |
| 2 | 0.0000 | 0.0000 | 0.0000 | 0.0000 | 0.0000 | 0.0000 | 0.0000 | 0.0000 | 0.0000 | 0.0000 | 0.0000 | 0.0000 |
| 3 | 0.0031 | 0.0031 | 0.0032 | 0.0032 | 0.0000 | 0.0000 | 0.0000 | 0.0000 | 0.0011 | 0.0011 | 0.0024 | 0.0024 |
| 4 | 0.0131 | 0.0162 | 0.0103 | 0.0135 | 0.0000 | 0.0000 | 0.0000 | 0.0000 | 0.0046 | 0.0057 | 0.0077 | 0.0101 |
| 5 | 0.0246 | 0.0408 | 0.0156 | 0.0292 | 0.0046 | 0.0046 | 0.0158 | 0.0158 | 0.0116 | 0.0173 | 0.0157 | 0.0257 |
| 6 | 0.0319 | 0.0727 | 0.0169 | 0.0461 | 0.0137 | 0.0183 | 0.0303 | 0.0552 | 0.0201 | 0.0373 | 0.0227 | 0.0484 |
| 7 | 0.0183 | 0.0910 | 0.0084 | 0.0545 | 0.0361 | 0.0544 | 0.0892 | 0.1443 | 0.0299 | 0.0672 | 0.0291 | 0.0775 |
| 8 | | | | | 0.0431 | 0.0975 | 0.0935 | 0.2378 | 0.0281 | 0.0952 | 0.0240 | 0.1014 |
| 9 | | | | | 0.0414 | 0.1389 | 0.0800 | 0.3178 | 0.0270 | 0.1222 | 0.0205 | 0.1219 |
| 10 | | | | | 0.0385 | 0.1775 | 0.0670 | 0.3849 | 0.0251 | 0.1473 | 0.0172 | 0.1391 |
| 11 | | | | | 0.0331 | 0.2105 | 0.0524 | 0.4373 | 0.0215 | 0.1688 | 0.0134 | 0.1525 |
| 12 | | | | | 0.0272 | 0.2378 | 0.0396 | 0.4769 | 0.0177 | 0.1865 | 0.0101 | 0.1627 |
| 13 | | | | | 0.0298 | 0.2675 | 0.0400 | 0.5168 | 0.0194 | 0.2059 | 0.0102 | 0.1729 |
| 14 | | | | | 0.0310 | 0.2985 | 0.0387 | 0.5555 | 0.0202 | 0.2261 | 0.0099 | 0.1828 |
| 15 | | | | | 0.0257 | 0.3242 | 0.0299 | 0.5855 | 0.0167 | 0.2428 | 0.0077 | 0.1905 |
| 16 | | | | | 0.0244 | 0.3487 | 0.0267 | 0.6122 | 0.0159 | 0.2587 | 0.0068 | 0.1973 |
| 17 | | | | | 0.0263 | 0.3750 | 0.0271 | 0.6393 | 0.0171 | 0.2758 | 0.0069 | 0.2043 |
| 18 | | | | | 0.0260 | 0.4010 | 0.0253 | 0.6646 | 0.0169 | 0.2927 | 0.0065 | 0.2108 |
| 19 | | | | | 0.0198 | 0.4208 | 0.0183 | 0.6829 | 0.0129 | 0.3056 | 0.0047 | 0.2154 |
| 20 | | | | | 0.0174 | 0.4382 | 0.0152 | 0.6981 | 0.0113 | 0.3169 | 0.0039 | 0.2193 |
| 21 | | | | | 0.0191 | 0.4573 | 0.0159 | 0.7141 | 0.0124 | 0.3293 | 0.0041 | 0.2234 |
| 22 | | | | | 0.0194 | 0.4767 | 0.0155 | 0.7296 | 0.0126 | 0.3420 | 0.0040 | 0.2274 |
| 23 | | | | | 0.0202 | 0.4969 | 0.0154 | 0.7450 | 0.0131 | 0.3551 | 0.0039 | 0.2313 |
| 24 | | | | | 0.0189 | 0.5158 | 0.0138 | 0.7588 | 0.0123 | 0.3674 | 0.0035 | 0.2349 |
| 25 | | | | | 0.0187 | 0.5345 | 0.0131 | 0.7719 | 0.0122 | 0.3796 | 0.0034 | 0.2382 |
| 26 | | | | | 0.0146 | 0.5491 | 0.0099 | 0.7817 | 0.0095 | 0.3891 | 0.0025 | 0.2408 |
| 27 | | | | | 0.0191 | 0.5681 | 0.0124 | 0.7941 | 0.0124 | 0.4015 | 0.0032 | 0.2439 |
| 28 | | | | | 0.0134 | 0.5815 | 0.0084 | 0.8025 | 0.0087 | 0.4102 | 0.0022 | 0.2461 |
| 29 | | | | | 0.0201 | 0.6016 | 0.0122 | 0.8147 | 0.0131 | 0.4233 | 0.0031 | 0.2492 |
| 30 | | | | | 0.0140 | 0.6156 | 0.0082 | 0.8229 | 0.0091 | 0.4324 | 0.0021 | 0.2513 |
| 31 | | | | | 0.0138 | 0.6294 | 0.0078 | 0.8307 | 0.0090 | 0.4413 | 0.0020 | 0.2533 |
| 32 | | | | | 0.0206 | 0.6500 | 0.0113 | 0.8420 | 0.0134 | 0.4547 | 0.0029 | 0.2562 |
| 33 | | | | | 0.0141 | 0.6641 | 0.0075 | 0.8496 | 0.0092 | 0.4639 | 0.0019 | 0.2581 |
| 34 | | | | | 0.0142 | 0.6784 | 0.0074 | 0.8569 | 0.0093 | 0.4732 | 0.0019 | 0.2600 |
| 35 | | | | | 0.0145 | 0.6929 | 0.0073 | 0.8642 | 0.0094 | 0.4826 | 0.0019 | 0.2619 |
| 36 | | | | | 0.0152 | 0.7080 | 0.0074 | 0.8716 | 0.0099 | 0.4925 | 0.0019 | 0.2638 |
| 37 | | | | | 0.2920 | 1.0000 | 0.1284 | 1.0000 | 0.1900 | 0.6825 | 0.0329 | 0.2967 |

AVERAGE MOLE WEIGHTS: OIL = 247.635 GAS = 45.779 HYDROCARBONS = 224.266 OVERALL = 97.486

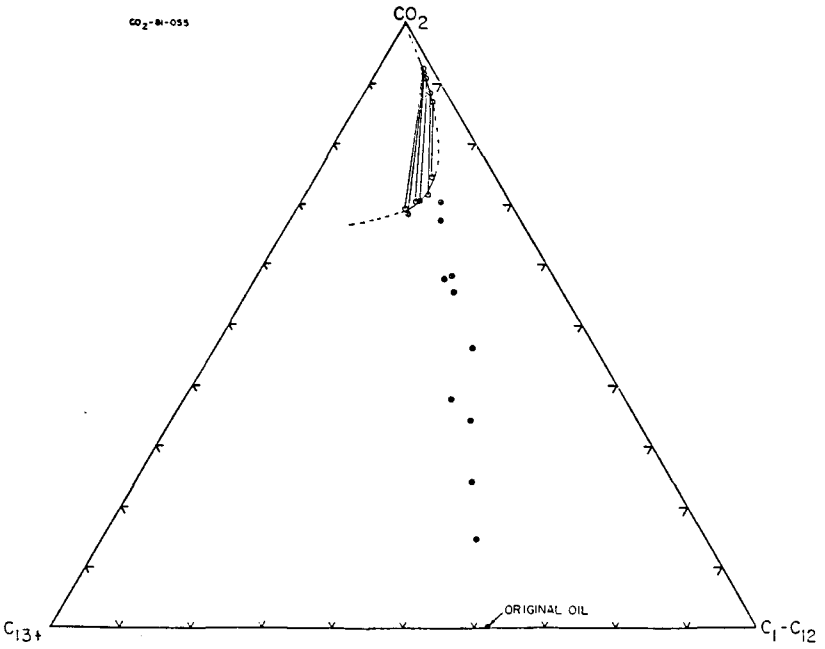


Fig. 2.15 Pseudo-ternary representation of phase compositions of mixtures of $CO_2$ with Maljamar separator oil at 1400 psia and 90°F.

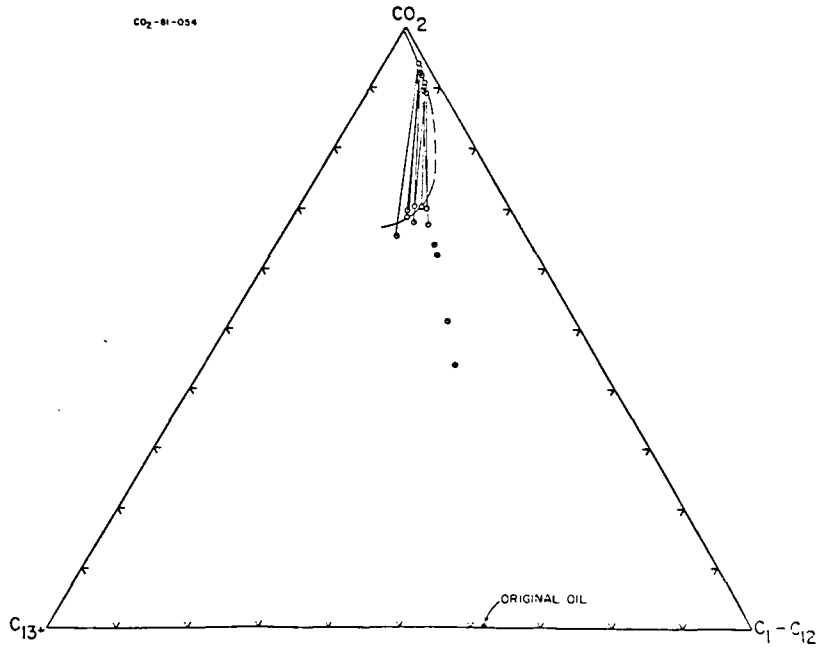


Fig. 2.16 Pseudo-ternary representation of phase compositions of mixtures of $CO_2$ with Maljamar separator oil at 1200 psia and 90°F.

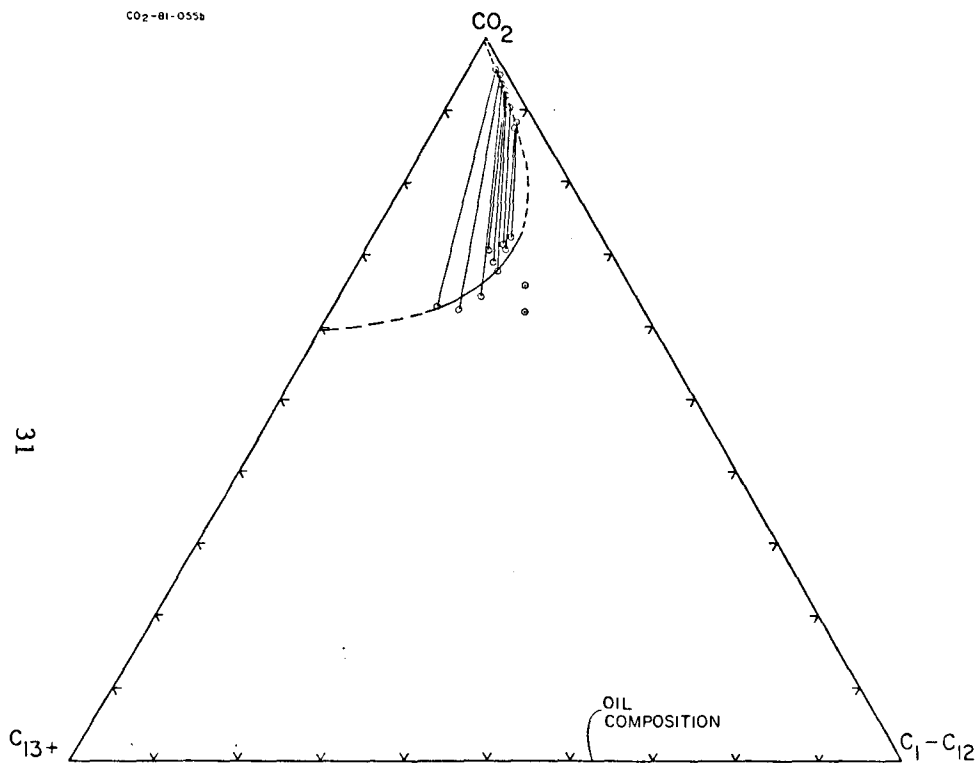


Fig. 2.17 Pseudo-ternary representation of phase compositions of mixtures of $CO_2$ with Rock Creek separator oil at 1300 psia and 75°F.

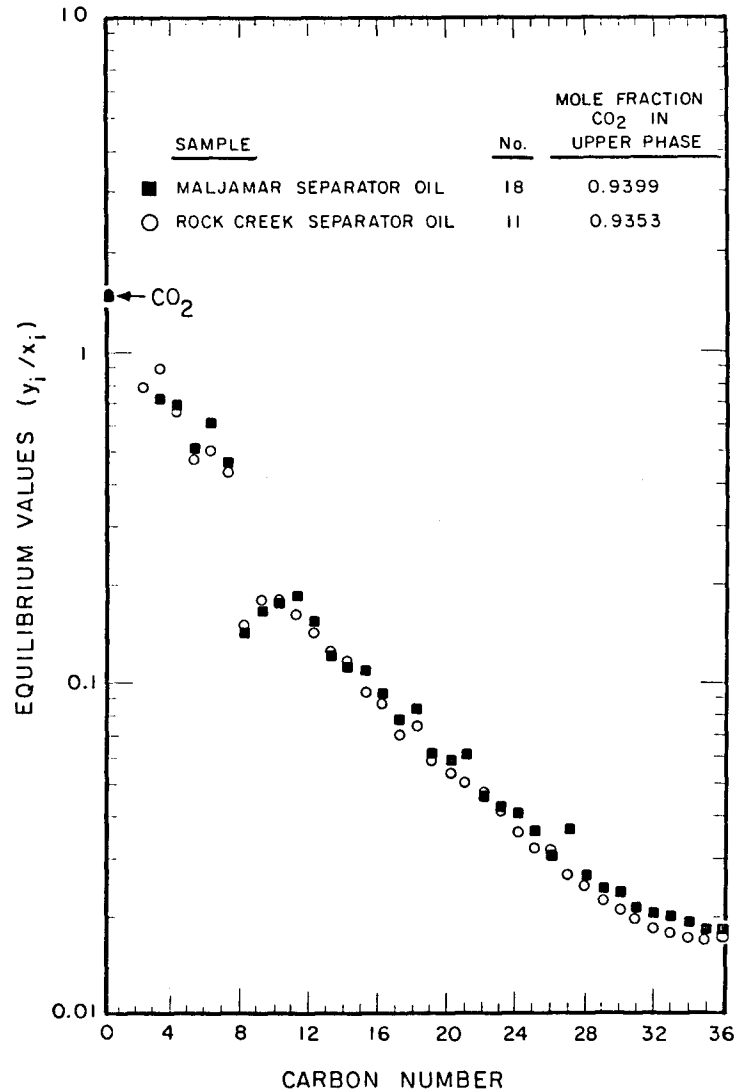


Fig. 2.18 Comparison of partition coefficients for Rock Creek and Maljamar crude oils mixed with $CO_2$.